

# Using Snowfall Intensity to Improve the Correction of Adjustments for Wind-Induced Undercatch in Solid Snowfall Measurements based on Precipitation Measurements Intensity

Matteo Colli<sup>1,2</sup>, Mattia Stagnaro<sup>2,3</sup>, Luca Lanza<sup>2,3</sup>, Roy Rasmussen<sup>4</sup> and Julie M. Thériault<sup>5</sup>

<sup>1</sup> Electrical, Electronics and Telecommunication Engineering and Naval Architecture Department, University of Genoa, Genoa, 16145, Italy

<sup>2</sup>WMO/CIMO Lead Centre “B. Castelli” on Precipitation Intensity, Genoa, 16145, Italy

<sup>3</sup>Department of Civil, Chemical and Environmental Engineering, University of Genoa, Genoa, 16145, Italy

<sup>4</sup>[Department of Earth and Atmospheric Sciences, Université du Québec à Montréal, Montreal, H2X 3Y7, Quebec, Canada](#)

<sup>5</sup>[Research applications Laboratory, National Center for Atmospheric Research\\*, Boulder, 80307-3000, Colorado, USA](#)

<sup>5</sup>[Department of Earth and Atmospheric Sciences, Centre ESCER, Université du Québec à Montréal, Montreal, H2X 3Y7, Quebec, Canada](#)

Correspondence to: Matteo Colli (matteo.colli@unige.it)

**Abstract.** ~~Transfer functions are generally used to adjust~~ Adjustments for the wind-induced undercatch of ~~solid precipitations~~ snowfall measurements. ~~These use transfer functions are derived based onto account for the variation expected reduction of the collection efficiency with increasing the wind speed for a particular catching-type of gauge, either using.~~ Based on field experiments or ~~based on~~ numerical simulation. ~~Most studies use the, collection efficiency curves as a function of wind speed alone, while others also include involve further explanatory variables such as surface air temperature and/or precipitation type to try to reduce the scatter.~~ However, while the wind speed or wind speed and temperature approach is generally effective at reducing the measurement bias, it does not significantly reduce the Root Mean Square Error (RMSE) of the residuals ~~at a given wind speed,~~ implying that part of the variance is still unexplained. In this study, we ~~propose the use of the measured~~ show that using precipitation intensity ~~to improve the effectiveness of~~ as the transfer function. ~~explanatory variable significantly reduces the scatter of the residuals.~~ This is achieved by ~~applying~~ optimized curve fitting ~~to of~~ field measurements from the Marshall field-test site (CO, USA). ~~The use of), using~~ a non-gradient optimization algorithm ~~ensures to ensure~~ optimal binning of experimental data ~~according to the parameter under test. The results reveal that using precipitation intensity as an explanatory variable significantly reduce the scatter of the residuals. The scatter reduction as indicated by the Root Mean Square Error (RMSE) is confirmed by the.~~ The analysis of ~~the~~ recent quality-controlled ~~data~~ dataset from the [WMO/SPICE Solid Precipitation InterComparison Experiment](#) campaign [of the World Meteorological Organization confirms the scatter reduction](#), showing that this approach ~~can be applied~~ is suitable to a variety of locations and catching-type gauges.

---

\* The National Center for Atmospheric Research is sponsored by the National Science Foundation

~~We Using Computational Fluid-Dynamics simulations, we demonstrate that the physical basis of the relationship between the collection efficiency and the measured reduction in RMSE is the correlation of precipitation intensity, due to the correlation of large particles with high intensities, by conducting a Computational Fluid-Dynamics (CFD) simulation. We use a Reynolds Averaged Navier-Stokes SST-k- $\omega$  model coupled with a Lagrangian particle-tracking model. Results validate the hypothesis of using the measured precipitation intensity as a key parameter to improve the correction of wind-induced undercatch.~~

~~Findings size distribution. Overall, these findings have the potential to improve operational measurements since no additional instrument other than a improved adjustments only require the use of the wind sensor is required to apply the correction. This improves the accuracy of precipitation measurements without the additional cost of ancillary instruments such as particle counters speed information.~~

## 1 Introduction

~~Precipitation In-situ liquid and solid precipitation measurements from commonly employ catching-type gauges are affected by instrumental and environmental errors. Amongst to collect hydrometeors while approaching the environmental factors ground surface. Factors affecting the capability of the gauge to collect and measure the actual precipitation occurring at a given site include wind, wetting, splashing, etc. (WMO, 2014). For a given gauge, we define the Collection Efficiency (CE) as the ratio between the precipitation amount  $P_{meas}$  (mm) measured by the gauge and the true precipitation  $P_{true}$  (mm):~~

$$CE = \frac{P_{meas}}{P_{true}}$$

~~In case of analytical or numerical models, the true precipitation is known, while it is generally unknown in the field for real world measurements. In this second case, it is common to replace  $P_{true}$  with a reference value  $P_{ref}$  obtained from high quality instruments and/or specific installations.~~

~~In case of snowfall measurements, wind plays a dominant role by in reducing the gauge collection ability, especially in case of solid precipitation efficiency (Goodison et al., 1998; Rasmussen et al., 2012). Nespor and Sevruk, 1999; Constantinescu et al.,~~

~~Over the past two decades, 2006 used Computational Fluid-Dynamic (CFD) simulations have been used to evaluate the wind-induced undercatch of traditional catching type gauges (rainfall). Nespor and Sevruk, 1999; Constantinescu et al., 2006; Thériault et al., (2012). used it for snowfall and compared the results with detailed observations of snow crystals. A recent analysis by Colli et al. (2015) showed good agreement between the collection efficiency predicted by time averaged models and of wind speed and particle trajectories and the field observations made at the NCAR/NOAA/FAA Marshall Field Test site (CO, USA, Rasmussen et al. 2012). In A shielded gauge in the latter case, the collection efficiency  $CE(-)$  is expressed as the~~

ratio between the precipitation amount measured by the tested gauge  $P$  (mm) and a Double Fence International Reference (DFIR) shielded gauge  $P_{DFIR}$  (mm) configuration provided the reference precipitation, since this reference system is designated as the international standard gauge shield configuration for snowfall measurement (Goodison et al. 1998).

Given the systematic nature of this environmental error, correction Adjustment methodologies (e.g. Yang et al., 1995) have been mainly based on establishing developed and are typically algebraic relationships between  $CE$  and the mean wind speed  $U_w$  ( $\text{msm s}^{-1}$ ), also referred to as transfer functions. Thériault et al. (2012) and Colli et al. (2015a) specified collection efficiency variation with  $CE$  curves as a function of wind speed for different solid precipitation types (following Rasmussen et al., 1999) and particle size distributions. (PSD). Wolff et al. (2015) proposed a sigmoidal variation of the collection with wind speed function for the  $CE$  using the observations collected in Haukeliseter (Norway), which). This relationship includes the environmental air temperature  $T$  ( $^{\circ}\text{C}$ ) as an additional parameter to take into account for the effect likely amount of water contained in the precipitation type. A recent paper by Kochendorfer et al. (2017a) describes a simplified inverse exponential formulation for the universal transfer function as follows:

$$CE = e^{-a(U_w)(1 - [\tan^{-1}(b(T)) + c])} \quad (1)$$

where  $a$ ,  $b$  and  $c$  are coefficients derived by fitting the field data. The analysis of Kochendorfer et al. (2017a,b) is based on measurements collected at the Marshall field site and highlighted that, while a transfer function can reduce the gauge's bias to near zero, a large RMSE still remains. Theriault et al (2012) suggest that the large RMSE is due to variability in the particle type and size distribution of solid precipitation. Another recent experiment conducted in Formigal (Spain) within the framework of the World Meteorological Organization (WMO) SPICE – Solid Precipitation InterComparison Experiment (Nitu et al., 2012) showed that “the impact of temperature and snowfall intensity on the catch ratio was less important than wind speed, but still noticeable (...)” (Buisan et al., 2016).

Colli et al. (2015) presented dry snow  $CE$  estimations for an unshielded and a single Alter (Alter, 1934) shielded gauges based on data from the Marshall field site. The comparison of CFD simulations and the observations (Figure 8 of Colli et al., 2015) highlights that a large part of the  $CE$  variability for a given wind speed is explained by the particle size distribution. Thériault et al. (2012 and 2015) reported that the catching performance of a shielded gauge is also significantly related to the vertical velocity of the particles approaching the gauge. The particle size distribution and vertical velocity contribute to the calculation of the measured snowfall intensity  $SI$  ( $\text{mmh}^{-1}$ ) as follows:

$$SI = \alpha \int_{D_{min}}^{D_{max}} N(D) \cdot w_p(D) \cdot D^3 dD \quad (2)$$

where  $D$  is the particle diameter (mm),  $N(D)$  the number of particles with diameter  $D$ ,  $w_p(D)$  their vertical velocity ( $\text{m s}^{-1}$ ) and  $\alpha$  a factor that accounts for the shape of the snowflake.

Given the challenges to decrease the RMSE of the collection efficiency variation with wind speed, the goal of this study is to show the dependence of the gauge collection efficiency on snowfall intensity. Previous studies (e.g. Folland, 1988; Nespor

and Sevruk, 1998), focused on liquid precipitation, specified the functional relationships between wind-induced undercatch and  $U_w$  for different rainfall rate classes. Following a similar approach, the here investigated formulation of  $CE$  is a modified version of the relationship proposed by Kochendorfer et al. (2017) obtained by substituting the air temperature with  $SI$  as follows:

$$CE = e^{-a(U_w)(1 - [\tan^{-1}(b(SI) + c])]} \quad (3)$$

5

where  $a, b$  and  $c$  are numerical best-fit coefficients.

This approach is first developed by considering snow gauge data collected at the Marshall (CO, USA), CARE (Canada) and Haukeliseter (Norway) field test sites. Second, the results are compared with CFD modelling.

10 ~~The measurements and the data processing method used to perform the field data analysis are presented in section 2. Section 3 reports on the observed correlation between  $CE$  and either the measured snowfall intensity or the environmental temperature. A description of the data binning optimization according to  $SI$  is also included. The influence of the chosen time average period for measurement on the collection efficiency is described in section 4. In section 5 the dependency between the  $CE$  and the measured snowfall intensity is investigated using CFD simulations with the aim of providing a physical basis for the correlation observed in section 3.~~

## 15 **2 Methodology of field data analysis**

### **2.1 Field data processing**

20 ~~The development and testing of new methodologies to retrieve the  $CE$  requires the availability of quality controlled meteorological measurements at high time resolution from a properly instrumented test bed. The solid precipitation measurements used in this study were collected by a single Alter and a DFIR shielded Geonor T200B with a 6 second sampling time at the Marshall field site (CO, USA, Rasmussen et al., 2012). This period covers the WMO SPICE data collection period and is characterized by the availability of ancillary data to support investigation into factors such as wind speed and precipitation intensity as well as high levels of data scrutiny and quality control. Ancillary data are collected every minute. The single Alter (SA) Geonor T200B gauge measurements are compared to those made by the DFIR shielded Geonor T200B gauge that was defined as the working automated reference for WMO-SPICE (Kochendorfer et al., 2017c).~~

25 ~~Wind speed is measured at 2 m above the surface using a propeller anemometer (Model 05103 Wind Monitor, RM Young) whereas the temperature is at 1.5 m above the surface using a fan aspirated (Model 076B Radiation Shield, Met One Instruments) platinum resistance thermometers (Model CS500 L, Campbell Scientific).~~

30 ~~GEONOR weighing gauges are based on vibrating wire technology. Noise in the output is due to environmental factors that cause oscillations of the measuring bucket. These effects have been limited by post processing the 6 sec gauge time series with a Gaussian Linear Time Invariant (LTI) filter characterized by a filtering window equal to 2 min and a standard deviation equal to 1 min. A correction of the vibrating wires sensitivity to the environmental temperature has been applied as well. In~~

addition, an automatic quality control has been performed to check the occurrence of missing data, decreasing trends or jumps in the precipitation time series and in consistent records among by the three vibrating wires of the Geonor T200B gauges (Reverdin, 2016).

The measured CE is expressed as the ratio between the precipitation amount measured by the tested gauge and a Double Fence International Reference (DFIR). For the sake of highlighting any dependency between the collection efficiency and the snowfall intensity measured by the uncorrected gauge, the analysis reported in Section 3 is focused on a subset of 30 min measurements made at the Marshall field site that have been selected and quality controlled by the WMO SPICE procedures described in Reverdin (2016) and Kochendorfer et al. (2017b). This time period is short enough to represent the time variability of precipitation type, temperature and wind speed, and not too long to exclude changes in meteorological conditions (Kochendorfer et al., 2017). On the other hand, the 30 min time period is considered long enough to accumulate snowfall amounts that can be measured by the snow gauges. Furthermore, the sample is composed exclusively by measurements performed when the reference (DFIR) precipitation amount is higher or equal to 0.25 mm over the 30 min interval to reduce the effects of measurement noise. The period considered by such dataset starts from October 2013 and ends on April 2015 and is composed by a total of 72 days of precipitation. A threshold for the environmental temperature at  $-2^{\circ}\text{C}$  has been adopted to avoid the occurrence of liquid precipitation (Colli et al., 2015) resulting in a dataset of 183 solid precipitation data.

The 30 min WMO SPICE measurements of the shielded gauges and ancillary sensors obtained at CARE (Canada) and Haukeliseter (Norway) have been processed as well. At the CARE field site, the wind speed and temperature measured at 2 m above ground were measured by a NWS425 anemometer and HMP155 thermometer (Vaisala). At the Haukeliseter field site, wind speed measurements performed at a 10 m level above the ground have been performed by a WindObserver II anemometer manufactured by Gill Instruments and environmental temperature is measured by a PT100 platinum resistance thermometer sensor. In order to study the CE trend as a function of the wind speed, we adopted the Kochendorfer et al. (2017a) approach that estimates the wind speed at the gauge height equal to  $U_{10m} \times 0.71$  by assuming a log wind vertical profile (Thom, 1975).

Because the snowfall type, particle size distribution and terminal velocity at a given location highly vary in time, shorter time periods were also tested. These are 1 min, 5 min, 10 min and 20 min time interval. The Meteorological Services (Matrosov et al., 2009; Gergely and Garrett, 2016) usually use 30 min or 60 min intervals. To investigate the influence of the sampling interval on the CE variation with wind speed, the 1 min datasets at the Marshall test site from January 2013 to April 2015 was aggregated to obtained the 5 min, 10 min and 20 min time intervals. The environmental temperature of  $-2^{\circ}\text{C}$  was used as well to account for solid precipitation only. The wind speed and temperature datasets were also averaged over the same time intervals. A lower snowfall rate measured by the DFIR was set to  $SI_{DFIR} < 0.5$  mm/h to avoid cases of light snow occurring at some of the sites. Under these conditions, the total dataset is composed of 29 precipitation events for a total of 6943 minutes of precipitation.

Finally, the field data are compared to CFD simulations performed by imposing the same wind speed and precipitation intensity conditions. This provides an independent confirmation of the conclusions obtained from the field measurements analysis.

## 2.2 CFD simulation framework

### 2.2.1 Airflow modelling

The flow field is generated basing on the airflow dataset computed and described by Colli et al. (2015) to solve the three dimensional equations for the airflow around the single Alter GEONOR T200B gauge system. The spatial domain of the shielded gauge was subdivided into 10.0 million hexahedral and polyhedral cells with different degrees of refinements close to the gauge/shield surface to reach numerical convergence. The time-averaged air velocity, turbulent kinetic energy and pressure fields were solved by means of a Reynolds-Averaged Navier-Stokes  $k-\omega$  SST model. A direct comparison between the single Alter shielded and an unshielded configurations (Figure 3 of Colli et al., 2015) confirmed the advantage of using a single Alter shield. This gauge shield configuration reduces the velocity magnitude in the region contained within the fence and hence the exposure of the gauge to the wind.

Note that the calculation assumes uniform and steady air velocity profiles upstream of the gauge. The role of boundary layer turbulence on CE is currently being analysed with more accurate time dependent models, such as Large Eddy Simulation, and preliminary results have been presented in Colli et al. (2016b).

### 2.2.2 Collection efficiency modelling

The trajectories of dry and wet snow particles in the flow field past the single Alter and unshielded GEONOR gauge using wet and dry particle definitions in Rasmussen et al. (2001) were computed for wind speeds between 1 and 8 m/s with a Lagrangian model (Colli et al. 2015).

The influence of the particle size distribution on the CE scattering was analysed by simulating several particle sizes. The particle size distribution of solid precipitation can be described using the gamma distribution as shown by Brandes et al. (2006):

$$N(D) = N_0 \cdot D^\mu \cdot D^{-\lambda+D} \quad (4)$$

where  $N_0$  is the scale parameter,  $\mu$  characterizes the curvature and  $\lambda$  the slope of the distribution. According to Brandes et al. (2006)  $\mu$  can be estimated by the following expression:  $\mu = 0.00499 \lambda^2 + 0.798 \lambda - 0.666$ . In this work we adopted a general intercept value equal to  $N_0 = 1.5 \cdot 10^6 \text{ mm}^{-1} \text{ m}^{-3}$  and a variable slope parameter between  $0.5 \text{ mm}^{-1} < \lambda < 1.5 \text{ mm}^{-1}$  (Brandes et al., 2006; Theriault et al., 2012). The estimation of CE is based on the particle counting technique described in Colli et al. (2016b), which adopts the following integral expression:

$$CE(U_w) = \frac{\int_0^{d_{pmax}} V_w(d_p) A_{inside}(d_p, U_w) N(d_p) d_p}{\int_0^{d_{pmax}} V_w(d_p) A_{gauge} N(d_p) d_p} \quad (5)$$

where  $A_{inside}(d_p, U_w)$  is the effective collecting area associated with the number of particles collected by the gauge and  $A_{gauge}(d_p, U_w)$  is the area associated with the entering particles in case of undisturbed airflow and  $V_w(d_p)$  the equivalent water volume.

### 5 ~~3~~ Results from the field data analysis

The empirical CE for the single Alter shielded gauge as a function of wind speed, when the snow accumulation is aggregated over a 30 min time interval, is shown in Figure 1. The two panels show the same CE data calculated from field measurements but colour coded according to the air temperature  $T$  (panel a) and to the snowfall intensity  $SI_{SA}$ , as measured by the single Alter shielded gauge (panel b). The clustering of the CE according to the  $SI_{SA}$  is evident. It is observed that, for a given wind speed  $U_w$ , different  $CE = P_{SA}/P_{DFIR}$  ratios may occur according to a specific  $SI_{SA}$ , with higher collection efficiency values observed when the gauge collects an higher snowfall intensity. This trend becomes more evident when the mean horizontal wind speed is higher than 2 m/s with a more relevant clustering of the data according to  $SI_{SA}$ .

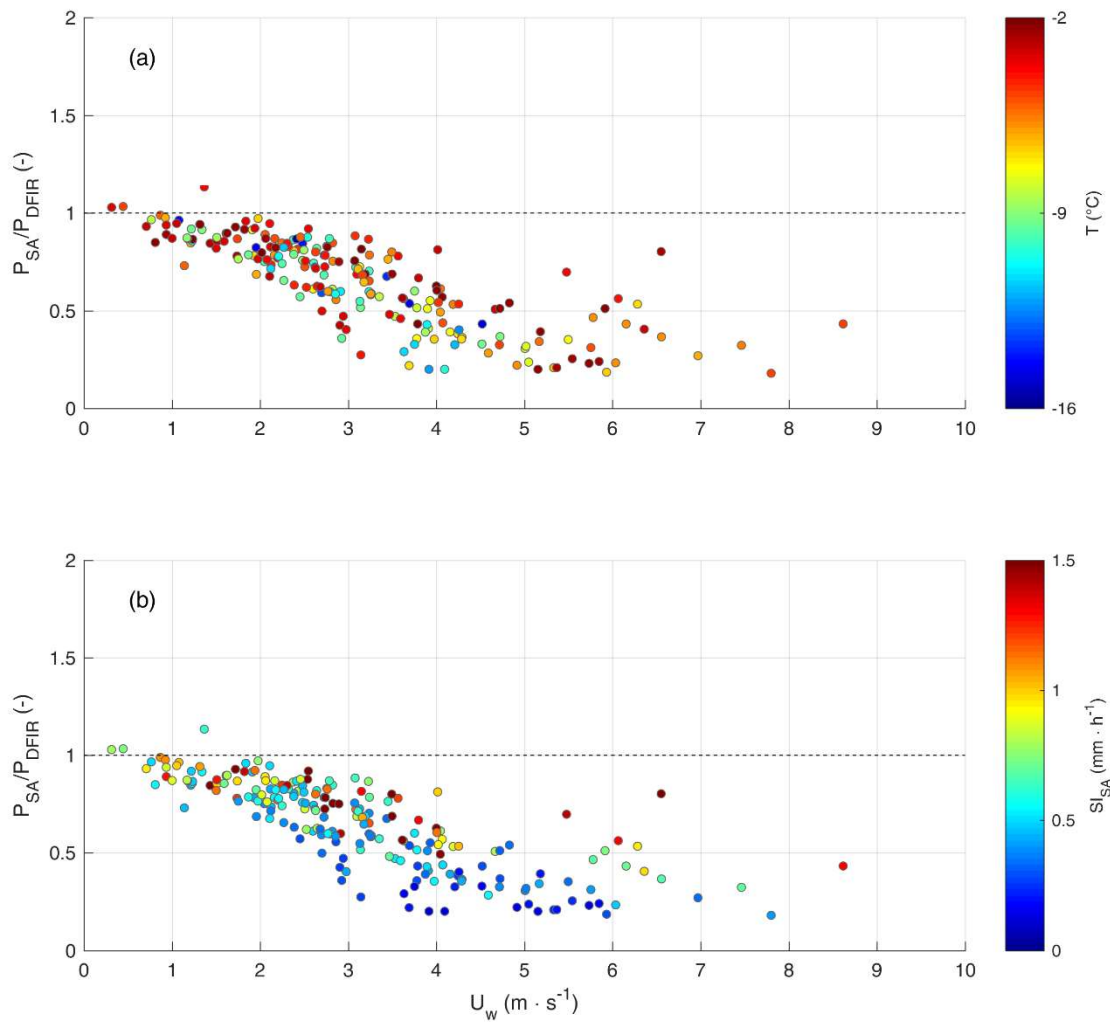


Figure 1: Collection efficiency  $CE=P_{SA}/P_{DFIR}$  for the 30-min single Alter gauge measurements from the Marshall field site in the period October 2013 to April 2015. Data points are colour coded according to the air temperature  $T$  (panel a) and the measured snowfall intensity  $SI_{SA}$  (panel b) showing the clustering of the measurements.

5

One explanation of the larger  $CE$  yielded by higher  $SI_{SA}$  of this trend is that the particles sizes are larger for higher snowfall intensities and, hence, less prone to be deflected by the deformed airflow above the gauge collector (Colli et al. 2016a,b). Thériault et al. (2012,2015) and Colli et al. (2015) showed a correlation between the slope parameter of the particle size distribution observed outside the tested gauge and its collection efficiency. Since low values of the slope mean larger particle sizes, this is consistent with the above suggestion.

10

In the following, the collection efficiency analysis is focused on the SPICE quality controlled 30 min dataset as used by Kochendorfer et al. (2017). A least squares regression of the inverse exponential function of  $CE(U_w, SI_{S,t})$  presented in equation 3 has been performed for the single Alter shielded gauge basing on the Marshall field site dataset together with the best fit obtained by equation 1 where the collection efficiency is expressed as a function of  $U_w$  and  $T$ . The coefficients obtained by the best fit analysis are listed in Table 1.

**Table 1: CE inverse exponential function coefficients ( $a$ ,  $b$  and  $c$ ), number of periods available ( $n$ ) and linear correlation coefficient ( $r$ ) for 30 min measurements made by the single Alter gauge at the Marshall (USA), CARE (Canada) and Haukeliseter (Norway) field sites from October 2013 to April 2015. The regression coefficients are calculated and compared for both  $CE(U_w, SI_{S,t})$  and  $CE(U_w, T)$  at each field site.**

<i>Field site</i>	<i>CE formulation</i>	<i>a</i>	<i>b</i>	<i>c</i>	<i>n</i>	<i>r</i>
Marshall (USA)	$CE(U_w, SI_{S,t})$	0.6737	12.8976	0.6589	183	0.91
	$CE(U_w, T)$	0.0520	0.1874	1.4971	183	0.82
CARE (Canada)	$CE(U_w, SI_{S,t})$	3.4531	107.4708	0.5835	234	0.85
	$CE(U_w, T)$	0.2892	0.0126	-0.7551	234	0.75
Haukeliseter (Norway)	$CE(U_w, SI_{S,t})$	0.4217	7.6856	0.7372	485	0.87
	$CE(U_w, T)$	0.5650	0.0198	-0.6711	485	0.75

The two regressions are presented in Figure 2. These are the  $CE(U_w, SI_{S,t})$  (panel a) and  $CE(U_w, T)$  (panel b) surfaces together with the field measurements (red points). The CE surfaces are colored according to the collection efficiency value and the  $CE(U_w, SI_{S,t})$  regression (panel b) shows a relevant dependency on the measured snowfall intensity together with the wind speed. Having selected a solid precipitation dataset according to the  $T < -2^\circ\text{C}$  threshold, the  $CE(U_w, T)$  regression represented in panel a shows a weak dependency to the environmental temperature  $T$ .

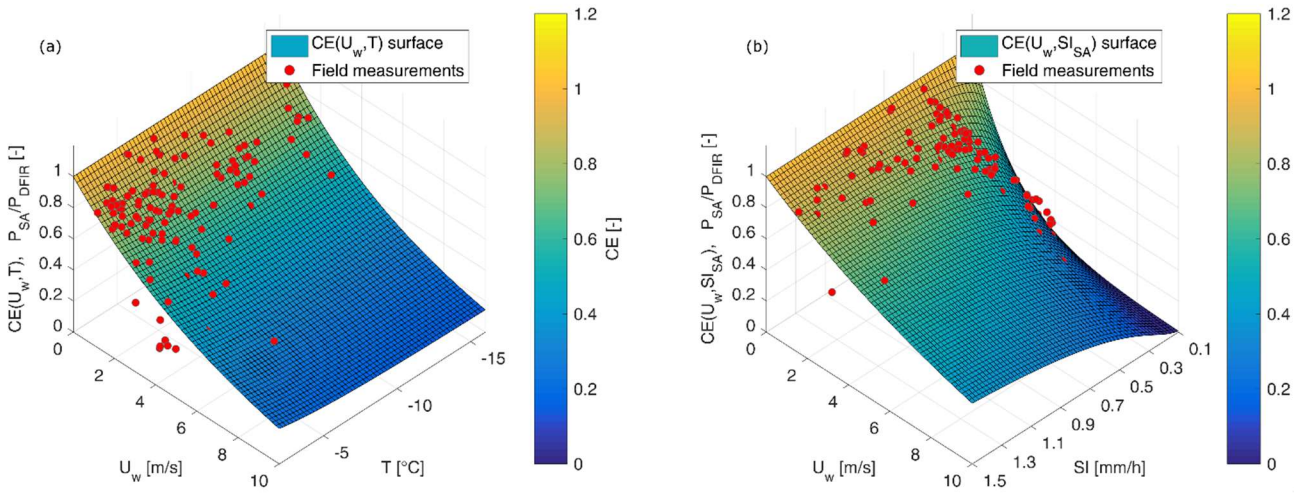


Figure 2: Collection efficiency  $CE = P_{SA}/P_{DFIR}$  of the 30-min single Alter gauge measurements made at the Marshall field site (red dots) and best-fit surfaces. Two regressions have been performed by expressing CE as a function of the wind speed  $U_w$  and either the air temperature  $T$  (panel a) or the measured snowfall intensity  $SI_{SA}$  (panel b).

- 5 In order to highlight the observed dependency between the CE and the snowfall intensity measured by the uncorrected gauge, Figure 3 presents  $CE(U_w, SI_{SA})$  plots for smaller subsets of field data selected according to the SI class. A non-gradient multi-objective genetic optimization algorithm, implemented in the DAKOTA open source toolkit (Eldred et al., 2007), was used to retrieve the best SI class limits (namely  $0.0 < SI_{SA} \leq 0.4 \text{ mm h}^{-1}$ ,  $0.4 < SI_{SA} \leq 0.6 \text{ mm h}^{-1}$ ,  $0.6 < SI_{SA} \leq 1.0 \text{ mm h}^{-1}$  and  $1.0 < SI_{SA} \leq 1.5 \text{ mm h}^{-1}$ ). The optimization objectives were to maintain a significant sample size for each bin and to minimize
- 10 the scatter of the CE values around their best fit curves (represented by the standard deviation of the residuals). The results show that each intensity category has a different fit to the sigmoid, with the lowest rates having the steepest decrease in collection efficiency with wind speed. This result is consistent with the highest intensities having the largest particles and therefore the smallest collection efficiency drops with wind speed.

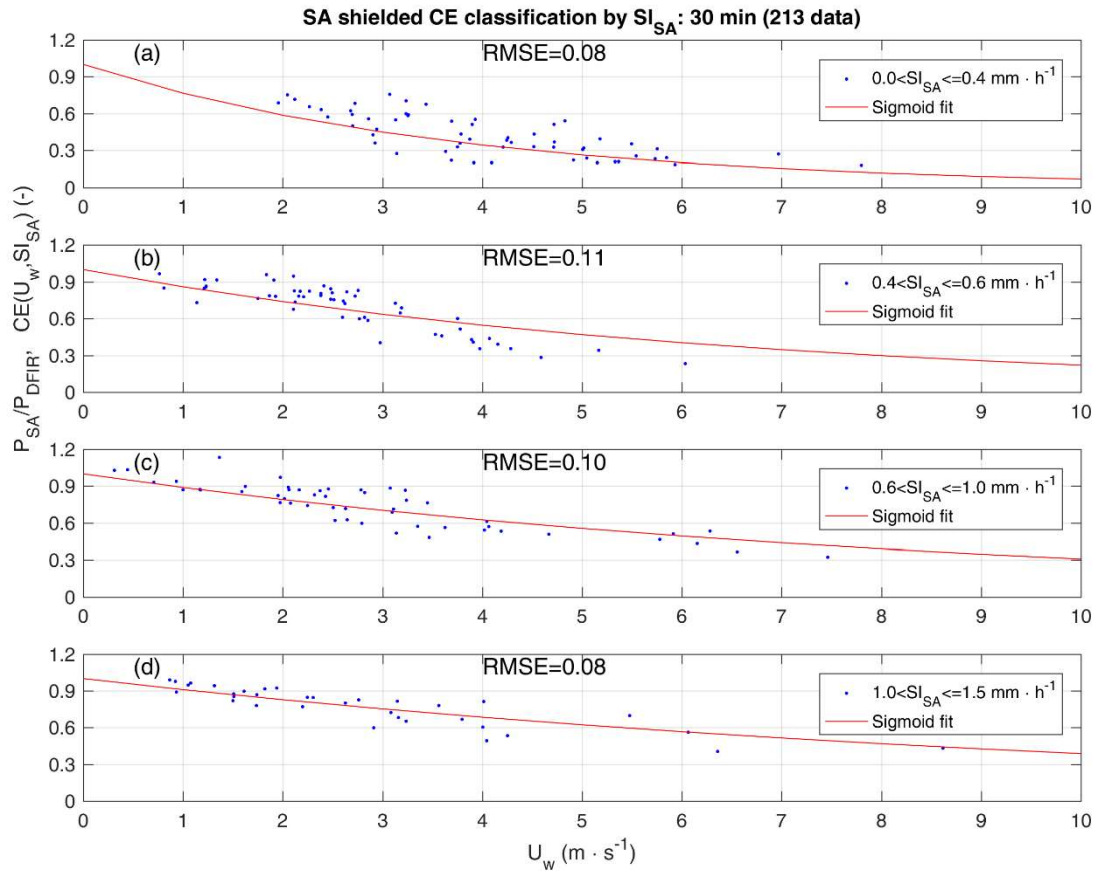


Figure 3: Empirical  $CE = P_{SA}/P_{DFIR}$  from measurements made by the single Alter snow gauge at the Marshall field site as a function of wind speed with a 30 min sampling interval. The solid line in each panel is the sigmoid best fit to the data. Each panel represents a different range of snow intensity ( $SI_{SA}$ ) as indicated by the key in the upper right of each panel and contains an evaluation of the RMSE of the residuals.

Wolff et al. (2015) and Colli et al. (2016b) showed that the influence of the type of precipitation on the catch performance of precipitation gauges could be taken into account by specifying the  $CE$  values according to the air temperature when considering the transition from snow to rain. The air temperature is an efficient indicator to ~~reeognized~~ determine the type of precipitation such as rainfall ( $T > 2^\circ\text{C}$  ~~from~~), wet snow ( $-2^\circ\text{C} < T < +2^\circ\text{C}$ ) and dry snow ( $T < -2^\circ\text{C}$ ) ~~eases but it~~. However, this is not representative of the large variety of ~~dry snow~~ crystal types ~~neither~~ and the ~~rimed snow~~ degree of riming (Rasmussen et al., 1999 and Thériault et al., 2012). ~~Figure 4 shows clearly that the scatter in the data is better represented by the  $SI$  rather than the air temperature. The four  $CE(U_w, T)$  curves show similar trends and nearly overlap each other demonstrating that there is~~

no significant correlation between the dry snow wind-induced undercatch and temperature below  $-2^{\circ}\text{C}$ . In contrast, the curves show a distinct separation when categorized by snowfall intensity for the 30-min dataset (Fig. 4, solid lines).

Recently, Kochendorfer et al. (2017a,b) described a simplified inverse exponential formulation for the universal transfer function using wind speed and air temperature. Their analysis is based on measurements collected at the Marshall field site and highlighted that a large Root Mean Square Error (RMSE) still remain even though a transfer function can reduce the gauge's bias to near zero. Thériault et al (2012) suggest using observations and simulations that the RMSE is due to the large variability in the particle type and size distribution of snowfall. The temperature can help determining the phase of the precipitation but not the size of hydrometeors, which helps explain the small impact of air temperature on the RMSE. Large uncertainties are also observed in the DFIR (Thériault et al., 2015) based on CFD simulations.

Further numerical simulations were conducted to study the fundamental processes leading to the large scatter in the data for a given wind speed. Colli et al. (2015) presented dry snow *CE* estimations for an unshielded and a Single Alter (SA) shielded gauges (Alter, 1934) based on data from the Marshall field site. The comparison of CFD simulations with the observations (Thériault et al., 2012; Colli et al., 2015) showed that a large part of the *CE* variability for a given wind speed is explained by the particle size distribution. Thériault et al. (2012; 2015) reported that the catch performance of a shielded gauge is also related to the particle's fall speed in the vicinity of the gauge.

These studies suggest that the particle type, size and the wind field can affect the gauge collection efficiency. To explore this further, we note that it is possible to represent the size distribution of precipitation particles by an inverse exponential function (Marshall and Palmer, 1948) that depends on two parameters, the slope and the intercept of its logarithmic representation. Pruppacher and Klett (1997) show that the slope of the PSD is closely related to the precipitation rate. As the precipitation rate increases, the slope of the size distribution decreases, leading to a higher concentration of large particles. Previous studies (e.g. Folland, 1988; Nespor and Sevruk, 1998), focusing on liquid precipitation only, specified the functional relationships between wind-induced undercatch and wind for different rainfall rate classes. Therefore, we suggest that the precipitation rate, i.e. snowfall intensity (SI), can be used to improve adjustments based on the *CE* curves. Such possibility is explored in this paper and shows to significantly reduce the RMSE.

Our method of investigation first considers precipitation gauge data collected at the Marshall (CO, USA), CARE (Canada) and Haukeliseter (Norway) field-test sites. Second, using CFD simulations, different PSDs are numerically tested and the *CE* is evaluated based on the associated precipitation intensity. This allowed testing the proposed hypothesis in a simplified environment where the noise that is typical of experimental datasets is avoided. The results show a good agreement of the *CE* values with field data and a clear dependency on the SI.

The measurements and the data processing method used to perform the field data analysis are presented in section 2.

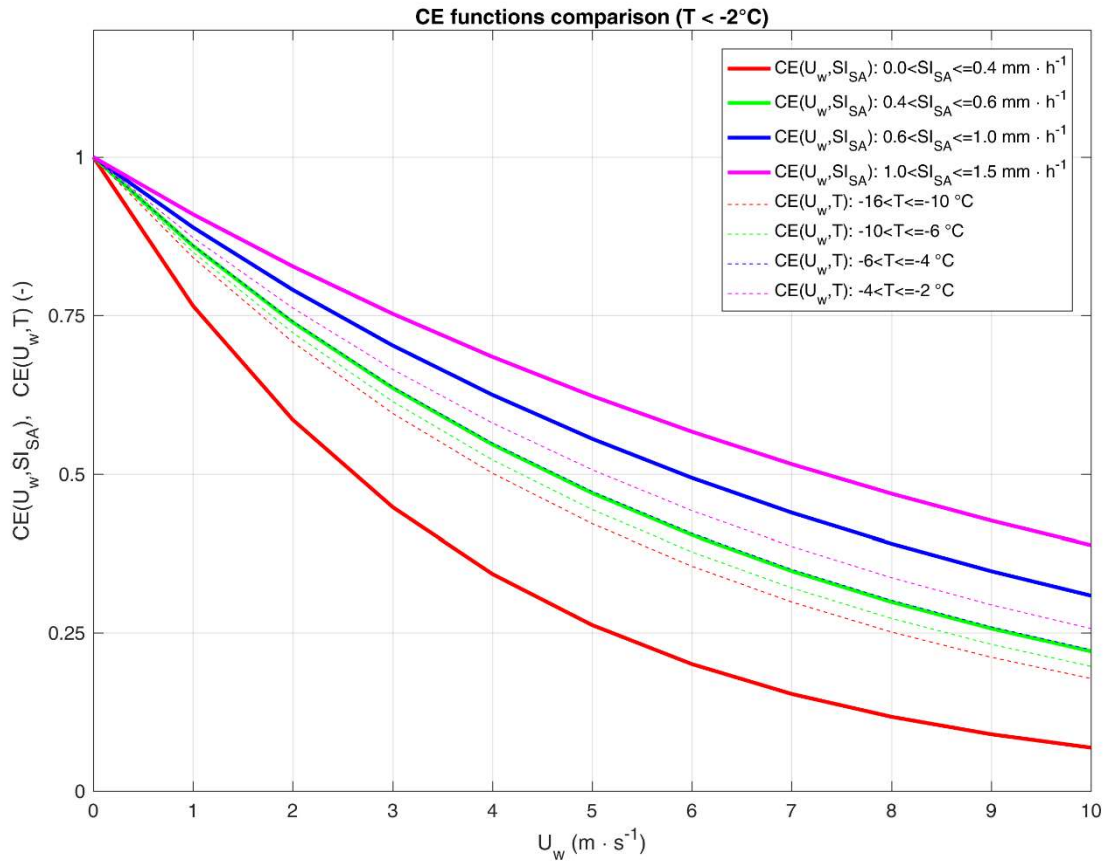


Figure 4:  $CE(U_w)$  curves of Section 3 reports on the observed correlation between  $CE$  and the measured  $SI$  or the environmental temperature. A description of the data binning optimization according to  $SI$  is also included. The influence of the chosen temporal aggregation of measurements on the derived  $CE$  is described in section 4. In section 5, the dependency between the  $CE$  and the measured  $SI$  is investigated using CFD simulations with the aim of providing a physical basis for the correlation observed in section 3.

## 2 Methodology of field data analysis

### 2.1 Field data processing

- 10 The development and testing of new methodologies to retrieve the  $CE$  requires the availability of quality controlled made by the single Alter snow, high frequency meteorological measurements from a properly instrumented test bed. The snowfall measurements used in this study were collected by two weighing gauge systems, one consisting of a Single Alter (SA) shield

surrounding a Geonor T200B weighing gauge with a 6-second sampling frequency and the second a DFIR shielded Geonor T200B. Both systems were co-located at the Marshall field site (CO, USA, Rasmussen et al., 2012) during 2013-2015 as part of the Solid Precipitation InterComparison Experiment program (SPICE) by WMO (Nitu et al., 2018). Ancillary data was also collected at the Marshall Field site every minute to support investigation into factors that might affect the *CE*. The SA Geonor T200B gauge measurements are compared to those made by the DFIR shielded Geonor T200B gauge, which was defined as the working automated reference for WMO-SPICE (Kochendorfer et al., 2017c).

Wind speed is measured 2 m above the ground surface using a propeller anemometer (Model 05103 Wind Monitor, RM Young) whereas the temperature was measured 1.5 m above the ground surface using a fan-aspirated (Model 076B Radiation Shield, Met One Instruments) platinum resistance thermometer (Model CS500-L, Campbell Scientific).

Geonor weighing gauges are based on vibrating wire technology. Noise in the output is typically due to environmental factors that cause oscillations of the measuring bucket. These effects have been reduced by post-processing the 6 s raw time series with a Gaussian linear time-invariant filter characterized by a filtering window equal to 2 min and a standard deviation equal to 1 min. A correction of the vibrating wires sensitivity to the environmental temperature has been applied as well. In addition, an automatic quality control was performed to check the occurrence of missing data, decreasing trends or jumps in the precipitation time series and inconsistent data from the three vibrating wires of the Geonor T200B gauge (Reverdin, 2016).

The measured *CE*, already defined in Section 1, is now better specified as the ratio between the precipitation amount measured by the SA shielded gauge ( $P_{SA}$ ) and the one measured by the DFIR shielded gauge ( $P_{DFIR}$ ), as follows:

$$CE = \frac{P_{SA}}{P_{DFIR}}$$

As for the Marshall field test site, we focused on the WMO-SPICE 30-min quality controlled site event data sets (SEDS), according to the procedure described in Reverdin (2016) and Kochendorfer et al. (2017b). Only 30-min data with reference precipitation ( $P_{DFIR}$ ) larger or equal to 0.25 mm were considered, for a total of 72 days of precipitation recorded from October 2013 to April 2015. The dataset was further reduced to consider events with an environmental temperature less than  $-2^{\circ}\text{C}$ , to avoid the occurrence of liquid precipitation (Colli et al., 2015), resulting in a final dataset of 213 30-min intervals (A-SEDS in Table 1).

The SEDSs from CARE (Canada) and Haukeliseter (Norway) were processed in a similar way and denoted B-SEDS and C-SEDS respectively in Table 1. At the CARE field site, the wind speed and temperature measured at 2-m above ground was measured by a NWS425 anemometer and HMP155 thermometer (Vaisala). At the Haukeliseter field site, wind speed measurements were made at 10 m level above the ground by a WindObserver II anemometer manufactured by Gill Instruments and a PT100 platinum resistance thermometer sensor measured the environmental temperature. We adopted the Kochendorfer et al. (2017a) approach to converting 10-m wind to 2-m gauge height wind. This entails correcting the 10 meter wind by a factor of 0.71;  $U_{10m} \times 0.71$ , assuming a logarithmic vertical profile of wind speed (Thom, 1975).

**Table 1: Location, measurement period, time interval and data consistency of SEDS (site event data set) considered in the analysis**

<u>Dataset</u>	<u>Location</u>	<u>Period</u>	<u>Time interval</u>	<u>N. of 30-min data</u>
<u>A</u>	<u>Marshall (CO-USA)</u>	<u>Jan. 2013 – Apr. 2015</u>	<u>1 min</u>	<u>6943</u>
<u>A-SEDS</u>	<u>Marshall (CO-USA)</u>	<u>Oct. 2013 – Apr. 2015</u>	<u>30 min</u>	<u>213</u>
<u>B-SEDS</u>	<u>CARE (Canada)</u>	<u>Nov. 2013 – Apr. 2015</u>	<u>30 min</u>	<u>234</u>
<u>C-SEDS</u>	<u>Haukeliseter (Norway)</u>	<u>Nov. 2013 – Apr. 2015</u>	<u>30 min</u>	<u>485</u>

Because the snowfall type, particle size distribution and terminal velocity at a given location are highly variable in time, shorter time intervals were also tested. Most meteorological services (Matrosov et al., 2009; Gergely and Garrett, 2016) use 30-min or 60-min intervals. To investigate the influence of the sampling interval on the  $CE$  variation with wind speed, the original 1-min dataset from the Marshall test site from January 2013 to April 2015 was aggregated to 5-min, 10-min and 20-min time intervals. The wind speed and temperature datasets were averaged over the same time intervals. A lower snowfall rate measured by the DFIR was set to  $SI_{DFIR} = 0.5$  mm/h to avoid cases of very light snow. Under these conditions, the total dataset – indicated as A in Table 1 – is composed of a total of 6943 one-minute samples recorded during 29 different precipitation events.

### **2.3 Data analysis method**

We analyse the  $CE$  as a function of wind speed and air temperature, as suggested by Wolff et al (2015) and Korchedoffer et al. (2017a), then we investigate the role of SI as an alternative explanatory variable. The SI is linked to the PSD and the vertical velocity of particles by the following equation:

$$SI = \alpha \int_{D_{min}}^{D_{max}} N(D) \cdot w_p(D) \cdot D^3 dD \quad (1)$$

where  $D$  is the particle diameter (mm),  $N(D)$  the number of particles with diameter  $D$ ,  $w_p(D)$  the vertical velocity ( $m s^{-1}$ ) and  $\alpha$  is a factor that accounts for the shape of the snowflakes.

The  $CE$  function suggested by Korchedoffer et al. (2017a) as a function of wind and the air temperature is expressed as:

$$CE = e^{-a(U_w)(1-[\tan^{-1}(b(T))+c])} \quad (2)$$

where  $U_w$  is wind velocity,  $T$  is the air temperature, while  $a$ ,  $b$  and  $c$  are empirical coefficients.

The role of the SI is tested using the following equation:

$$CE = e^{-a(U_w)(1-[\tan^{-1}(b(SI))+c])} \quad (3)$$

where  $a$ ,  $b$  and  $c$  are numerical best-fit coefficients. Equation (2) takes into account the precipitation phase while equation (3) takes into account the size of the hydrometeors.

### 3 Results from the field data analysis

grouped by the environmental temperature  $T$  (dashed lines) and the measured The empirical  $CE$  for the SA shielded gauge as a function of wind speed is shown in Figure 1 using the 30-min dataset A-SEDS. In the two panels,  $CE$  data are colour coded according to the air temperature  $T$  (panel a) and to the snowfall intensity  $SI_{SA}$  (panel b). No significant correlation is visually evident in panel a, while panel b shows a distinct cluster of low precipitation rates at low  $CE$ . While for any given wind speed, different  $CE$  may occur depending on the  $SI_{SA}$ , there is a higher  $CE$  observed when the gauge collects the higher  $SI$ . This trend becomes more evident when the mean horizontal wind speed is higher than 2 m/s.

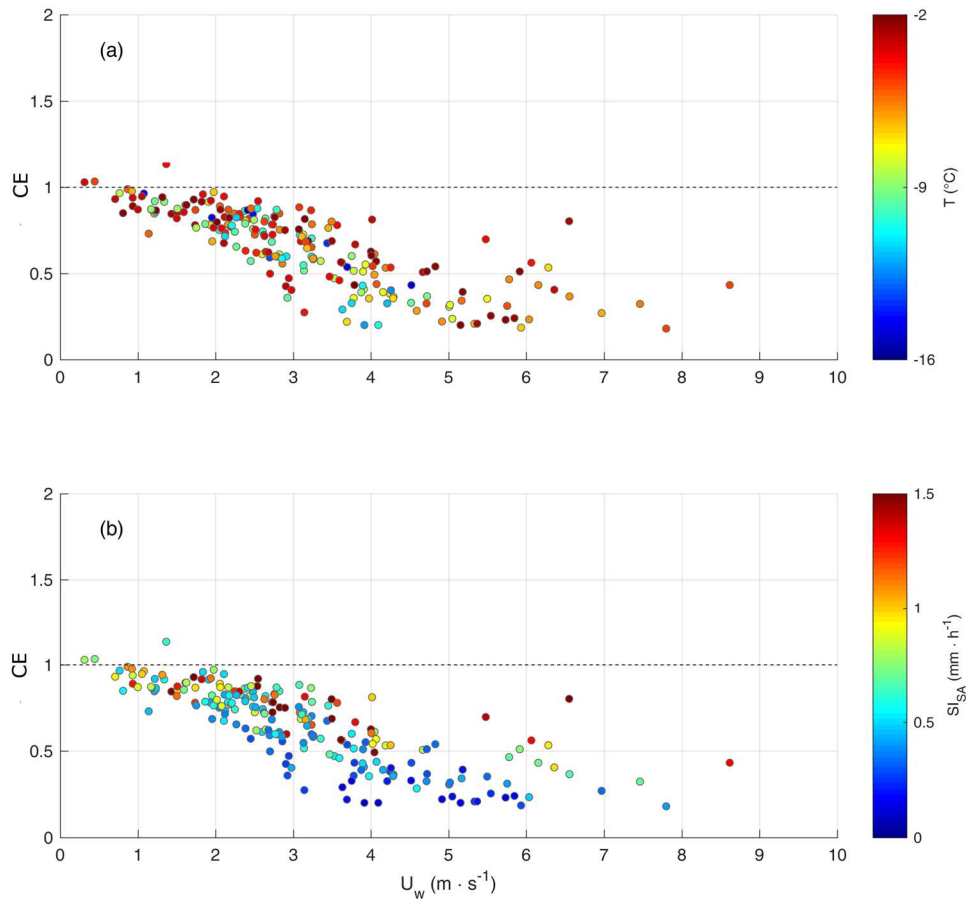


Figure 1: Collection efficiency  $CE=P_{SA}/P_{DFIR}$  for the 30 min SA shielded gauge measurements from the Marshall field site in the period October 2013 to April 2015. Data are colour coded according to the air temperature  $T$  (panel a) and the measured snowfall intensity  $SI_{SA}$  (panel b).

One explanation of the larger  $CE$  is related to larger particle sizes having trajectories that are less prone to deflection by the deformed airflow above the gauge collector (as detailed in Thériault et al., 2012 for different crystal types and by Colli et al. 2016a,b). Colli et al. (2015) showed a correlation between the slope parameter of the  $PSD$  outside the tested gauge and its  $CE$  by means of CFD analysis and the results were supported by disdrometers field data. Larger particles are associated with lower slope of the  $PSD$  and therefore higher  $SI$  (Pruppacher and Klett, 1997).

A least squares regression was performed on the inverse exponential function of the  $CE$  based on wind speed and temperature (Eq. 2) and the one based on wind speed and  $SI$  (Eq. 3). The coefficients obtained from the best-fit analysis are listed in Table 2.

**Table 2: Best-fit coefficients  $a$ ,  $b$  and  $c$  of the inverse exponential function, number of 30-min intervals used ( $n$ ) and linear correlation coefficient ( $R$ ) based on measurements made by the SA shielded gauge at the Marshall (USA), CARE (Canada) and Haukeliseter (Norway) field test sites from October 2013 to April 2015. Coefficients are calculated for both the  $CE(U_w, SI_{SA})$  and  $CE(U_w, T)$  at each field test site.**

<u>Field test site</u>	<u>CE formulation</u>	<u><math>a</math></u>	<u><math>b</math></u>	<u><math>c</math></u>	<u><math>n</math></u>	<u><math>R</math></u>
<u>Marshall (USA)</u>	<u><math>CE(U_w, SI_{SA})</math></u>	<u>0.6737</u>	<u>12.8976</u>	<u>0.6589</u>	<u>213</u>	<u>0.91</u>
	<u><math>CE(U_w, T)</math></u>	<u>0.0520</u>	<u>0.1874</u>	<u>1.4971</u>	<u>213</u>	<u>0.82</u>
<u>CARE (Canada)</u>	<u><math>CE(U_w, SI_{SA})</math></u>	<u>3.4531</u>	<u>107.4708</u>	<u>0.5835</u>	<u>234</u>	<u>0.85</u>
	<u><math>CE(U_w, T)</math></u>	<u>0.2892</u>	<u>0.0126</u>	<u>-0.7551</u>	<u>234</u>	<u>0.75</u>
<u>Haukeliseter (Norway)</u>	<u><math>CE(U_w, SI_{SA})</math></u>	<u>0.4217</u>	<u>7.6856</u>	<u>0.7372</u>	<u>485</u>	<u>0.87</u>
	<u><math>CE(U_w, T)</math></u>	<u>0.5650</u>	<u>0.0198</u>	<u>-0.6711</u>	<u>485</u>	<u>0.75</u>

The two regressions are presented in Figure 2. These are the  $CE(U_w, SI_{SA})$  (panel a) and  $CE(U_w, T)$  (panel b) surfaces together with the field measurements (red solid lines) with a 30-min accumulation time dots). The  $CE$  surfaces are colour-coded. The  $CE(U_w, SI_{SA})$  regression (panel b) shows a relevant dependency on the measured snowfall intensity. In contrast, the  $CE(U_w, T)$  regression represented in panel a shows a weaker dependency to the environmental temperature  $T$  than with the  $SI$ .

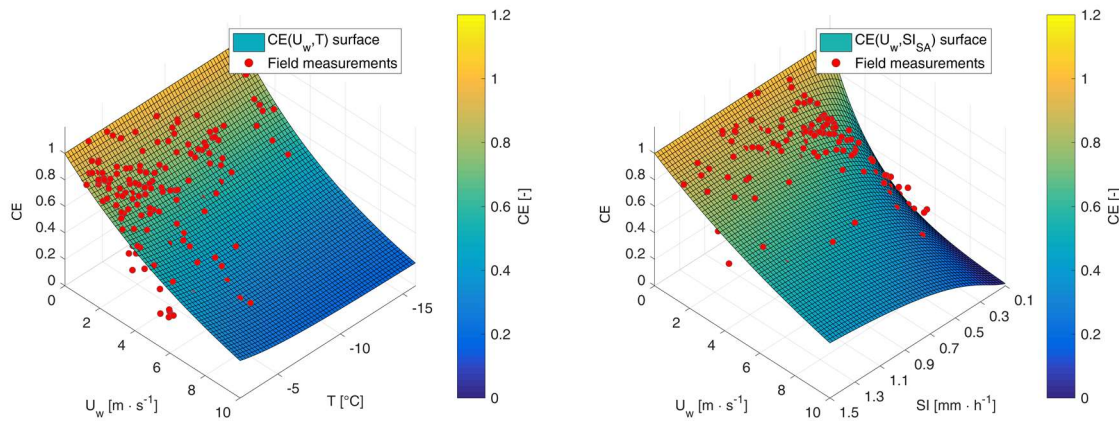


**Figure 2: Best-fit  $CE$  surfaces for the 30-min SA shielded snow gauge measurements made at the Marshall field test site (red dots). Two regressions are shown by expressing  $CE$  as a function of the wind speed and either the air temperature  $T$  (panel a) or the measured snowfall intensity  $SI_{SA}$  (panel b).**

To ensure optimal regression of the observed dependency between the  $CE$  and the  $SI$  measured by the uncorrected gauge, a non-gradient multi-objective genetic optimization algorithm, implemented in the DAKOTA open source toolkit (Eldred et al., 2007), was used to retrieve the best  $SI$  class limits. The following classes were obtained:  $0.0 < SI_{SA} \leq 0.4 \text{ mm h}^{-1}$ ,  $0.4 < SI_{SA} \leq 0.6 \text{ mm h}^{-1}$ ,  $0.6 < SI_{SA} \leq 1.0 \text{ mm h}^{-1}$  and  $1.0 < SI_{SA} \leq 1.5 \text{ mm h}^{-1}$ . The optimization objectives were to maintain a significant sample size for each bin and to minimize the scatter (RMSE) of the residuals. Figure 3 presents  $CE(U_w, SI_{SA})$  plots for smaller subsets of field data according to the optimised  $SI$  classes. The results show that each intensity category has a different fit to a sigmoid function, with the lowest  $SI$  class having the steepest decrease in  $CE$  with increasing wind speed. This is again explained by the highest intensities being associated with the largest particles, therefore slowly decreasing their  $CE$  with wind speed.

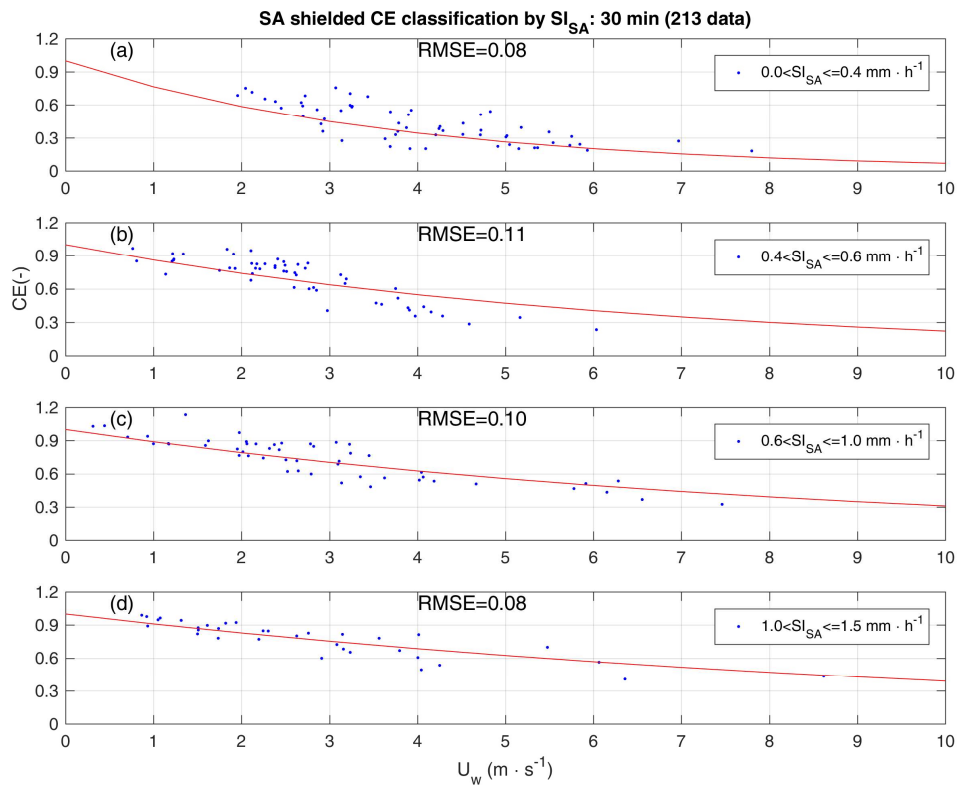


**Figure 3: Empirical  $CE$  for the 30-min SA shielded snow gauge measurements made at the Marshall field test site as a function of wind speed. The solid line in each panel is the sigmoidal best fit to the data. Each panel represents a different  $SI$  range as defined in the legends and reports the RMSE of the residuals.**

Figure 4 compares best-fit  $CE$  curves computed as a function of wind speed and either temperature or the  $SI$ . It shows that there is evidence of much stronger dependence on the  $SI$  classification (solid lines) than on temperature (dotted lines). The four  $CE(U_w, T)$  curves (dashed lines) show similar trends and are very close to each other, demonstrating that there is no significant correlation of the  $CE$  with temperature below  $-2^\circ\text{C}$ . In contrast, the curves show a distinct separation when categorized by  $SI$  for the 30-min dataset (solid lines).

5

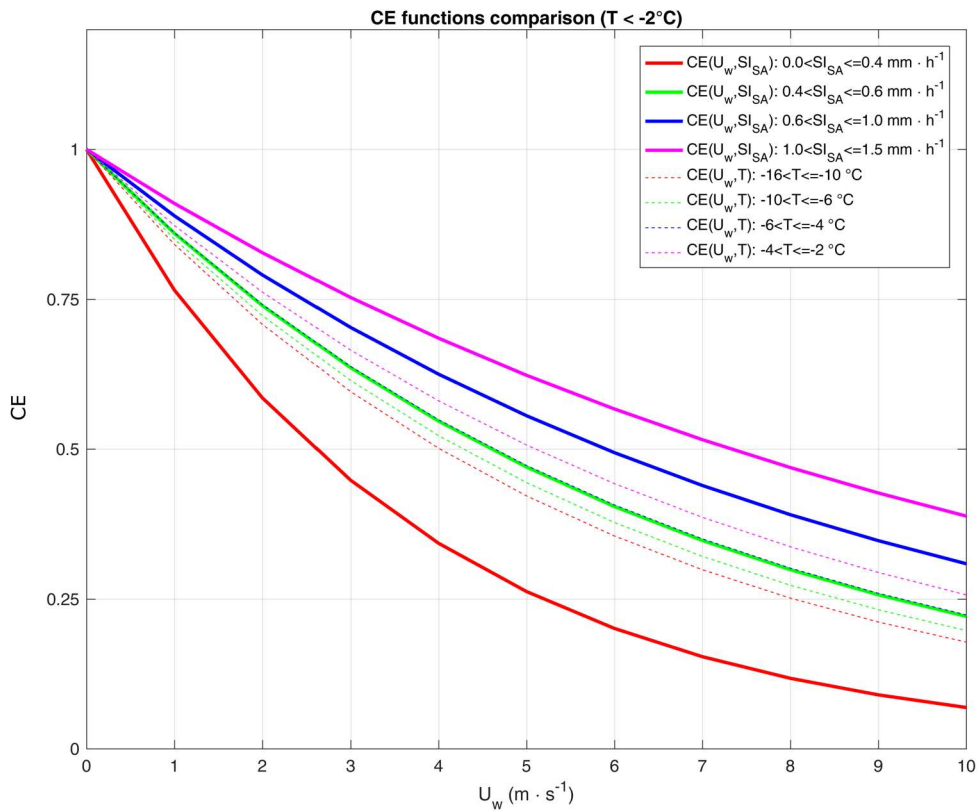
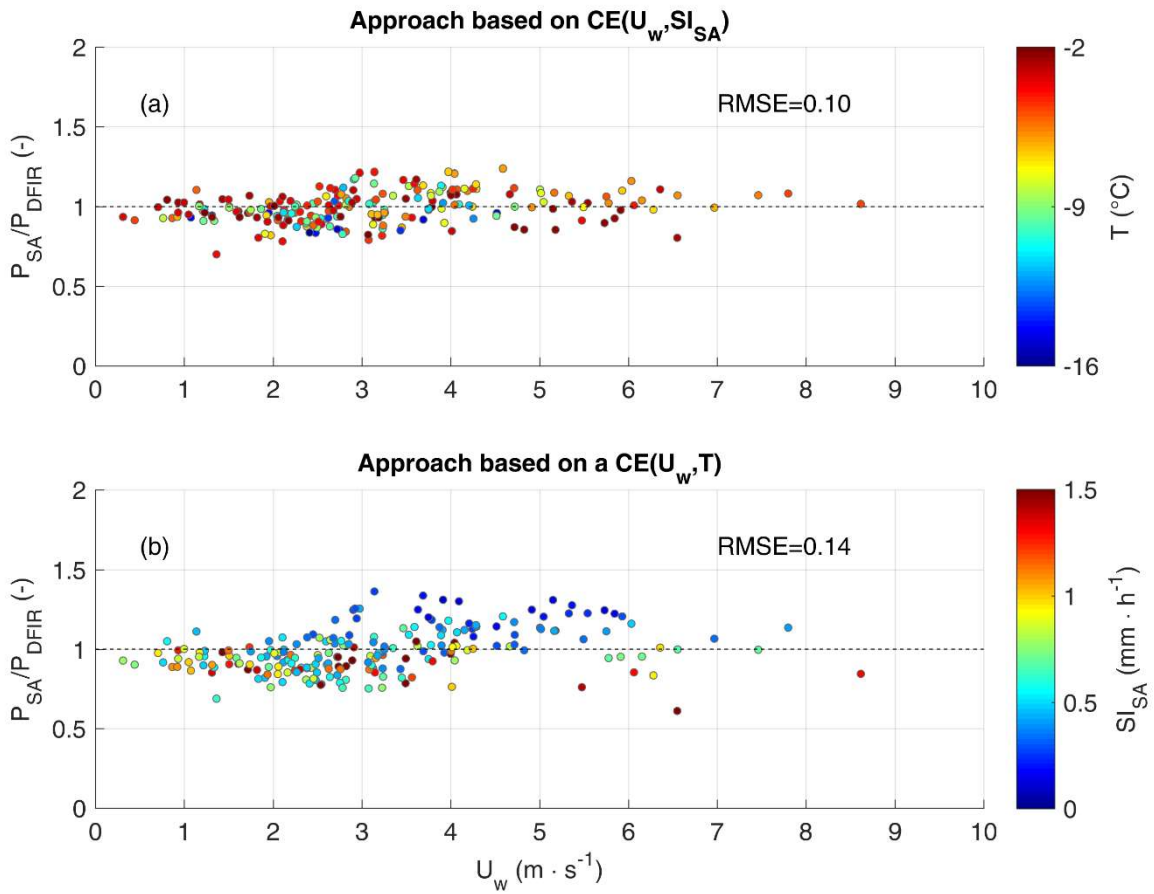


Figure 4: Best-fit  $CE$  curves of the 30-min measurements made by the SA shielded snow gauge at the Marshall field test site using either the air temperature  $T$  (dashed lines) or the measured  $SI$  (solid lines).  $SI$  curves are the same as in Figure 3.

An evaluation of the improvement to the improved snowfall accumulation estimates when using the intensity  $SI$  dependent curve fit is shown in Figure 5a, which represents where the corrected  $CE$  is shown and the associated root mean square error ( $RMSE$ ). The field data fall about a  $CE$  of 1.0 and the residuals is reported. The residual scattering is quantified by a  $RMSE$  equal to 0.10. The and the colour coded distribution of based on the environmental temperature on the corrected  $CE$  appears quite random. A larger scatter ( $RMSE=0.14$ ) is observed when the measurements are corrected by using wind speed and temperature (Fig. Figure 5b, traditional approach). Note that Figure 5b shows a colour separated dependence of the residuals

10

on the  $SI$ , indicating that notwithstanding the  $CE(U_w, T)$  correction some form of dependency persists between the SA shielded gauge undercatch and the characteristics of precipitation.



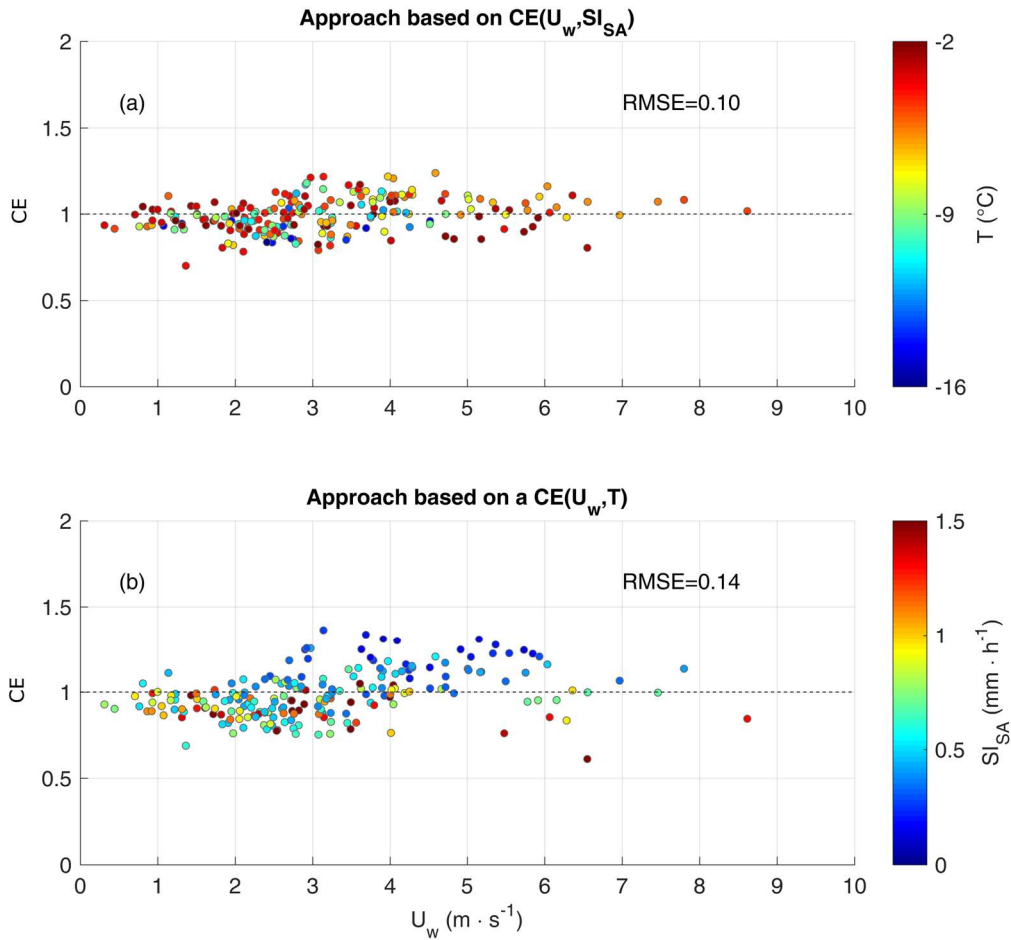


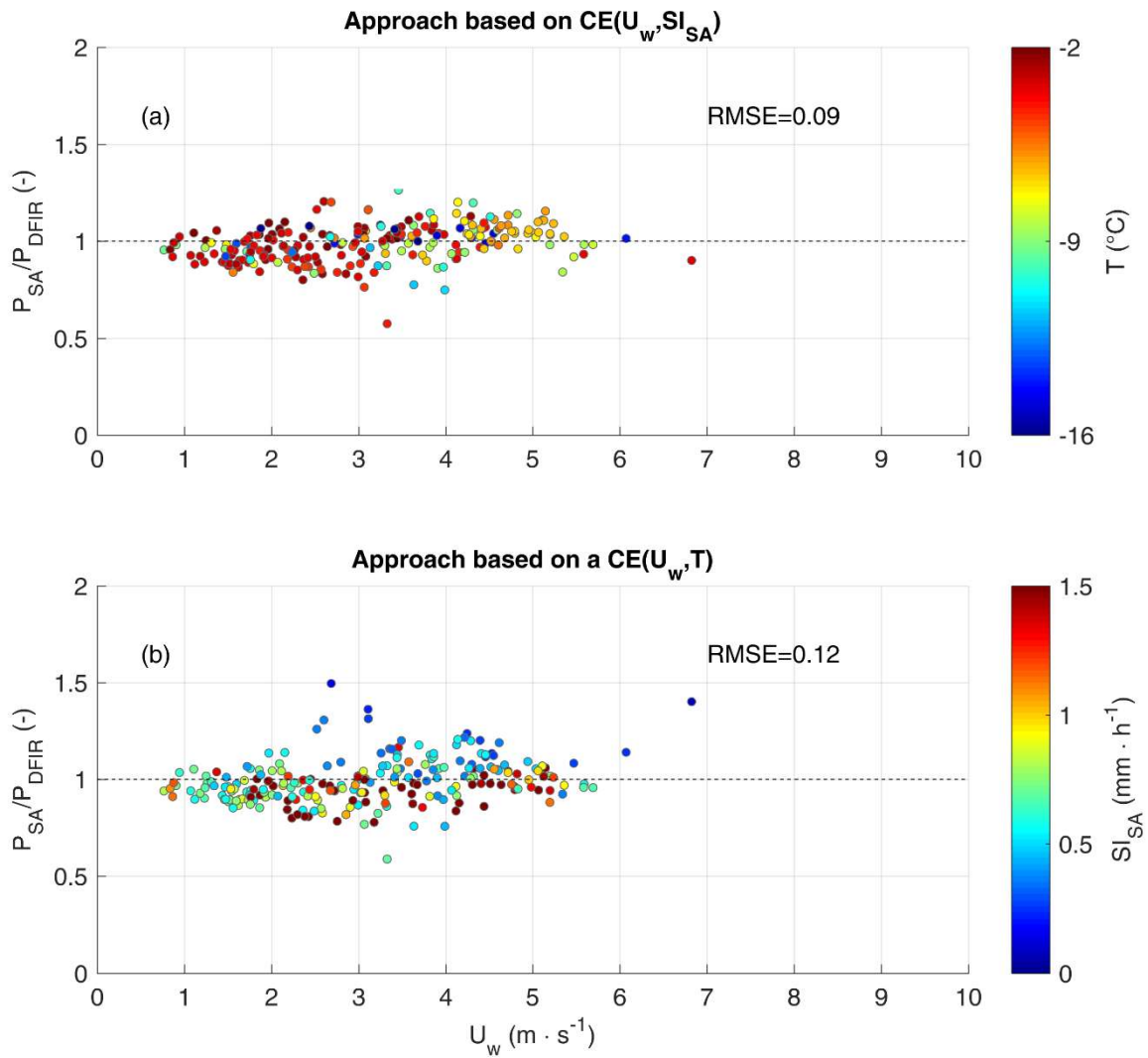
Figure 5: Residuals of  $CE = P_{SA}/P_{DFIR}$  obtained after correcting the 30-min single AlterSA shielded snow gauge measurements from the Marshall field test site using Equation 3 (top panel) and Equation 12 (bottom panel), with the associated RMSE values. Residuals are colour coded according to the environmental temperature  $T$  (top panel) and the snowfall intensity  $SI_{SA}$  (bottom panel).

5

Note that Figure 5b shows a colour separated dependence on wind speed, indicating that the  $CE(U_w, T)$  approach does not exploit all the forms of dependency between the accumulated precipitation measured by the single Alter shielded gauge and the characteristics of the precipitation events.

The best fit coefficients of the collection efficiency regression obtained with the CARE and Haukeliseter datasets are reported in Table 42 for both the  $CE(U_w, T)$  and  $CE(U_w, SI_{SA})$  formulations. The correction of the measurements based on such transfer functions is shown on Figure in Figures 6 and 7. The RMSEs of the residuals for the CARE measurements are equal to 0.09 in the case of  $CE(U_w, SI_{SA})$  and 0.12 in the case of  $CE(U_w, T)$  while the residuals for the Haukeliseter measurements show RMSEs that are equal respectively to 0.16 and 0.22. These RMSE results confirm that a correction the approach based

on the wind speed and precipitation intensity  $SI$  leads to a higher precision an improved correction of the solid precipitation measurements compared to when only the wind speed and. The results of the field data analysis suggest that the environmental temperature are can be used to provide an approximated criterion to recognize the precipitation phase (liquid, mixed or solid) while the  $SI$  is a more efficient explanatory variable since it is directly related to the  $PSD$ .



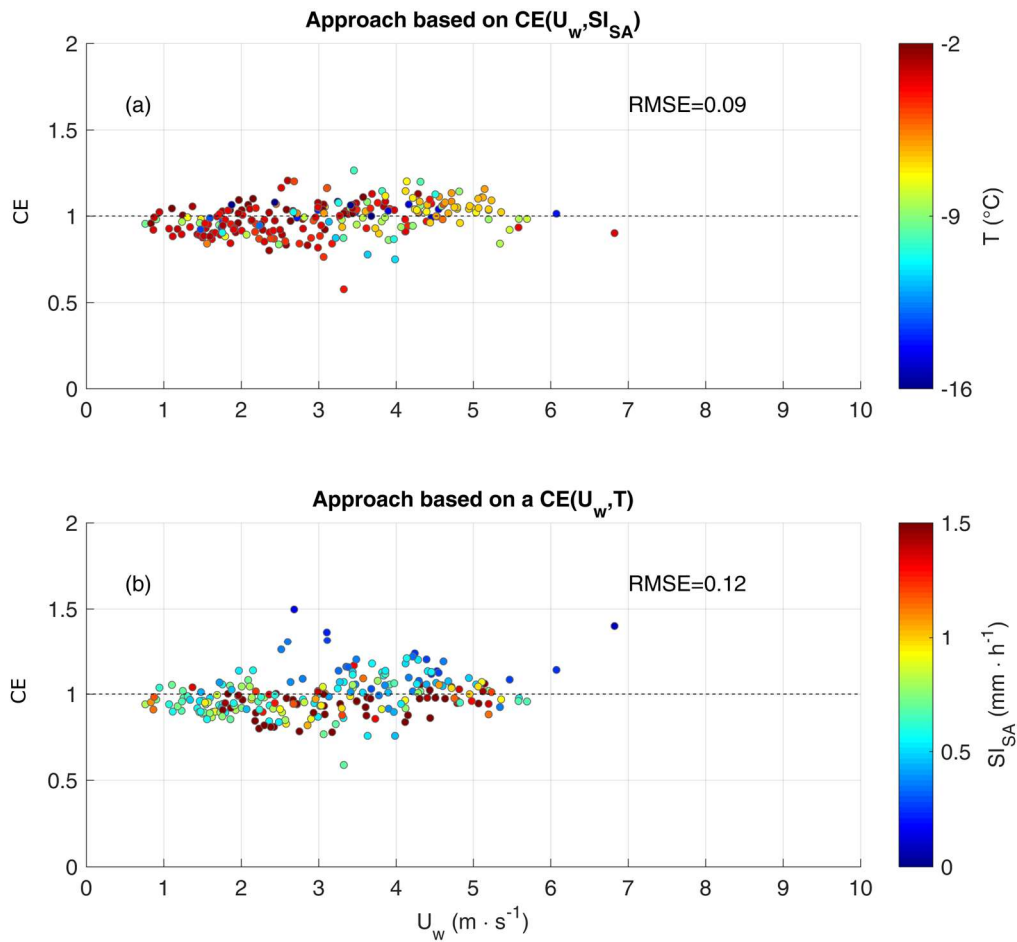
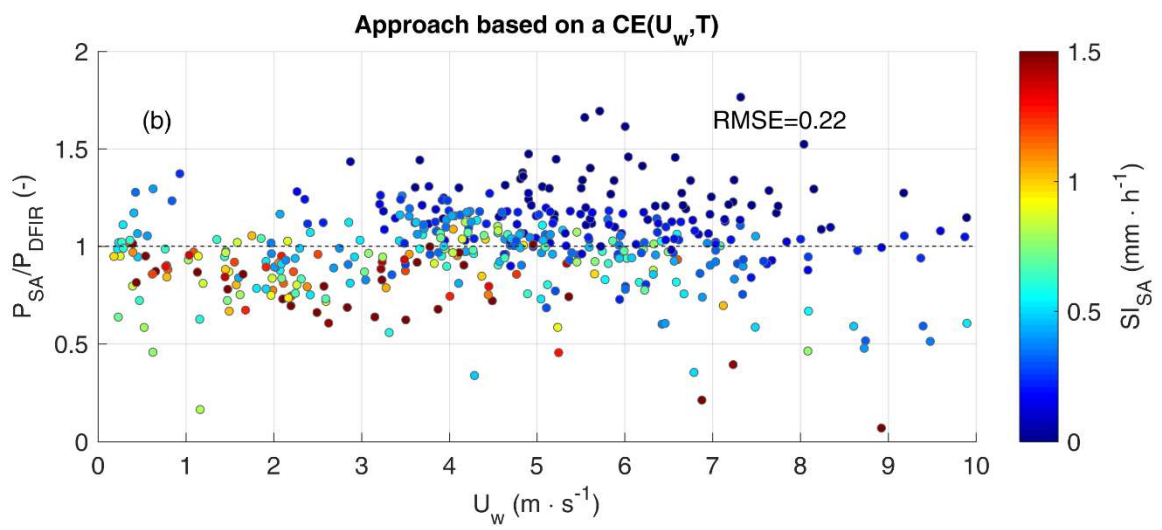
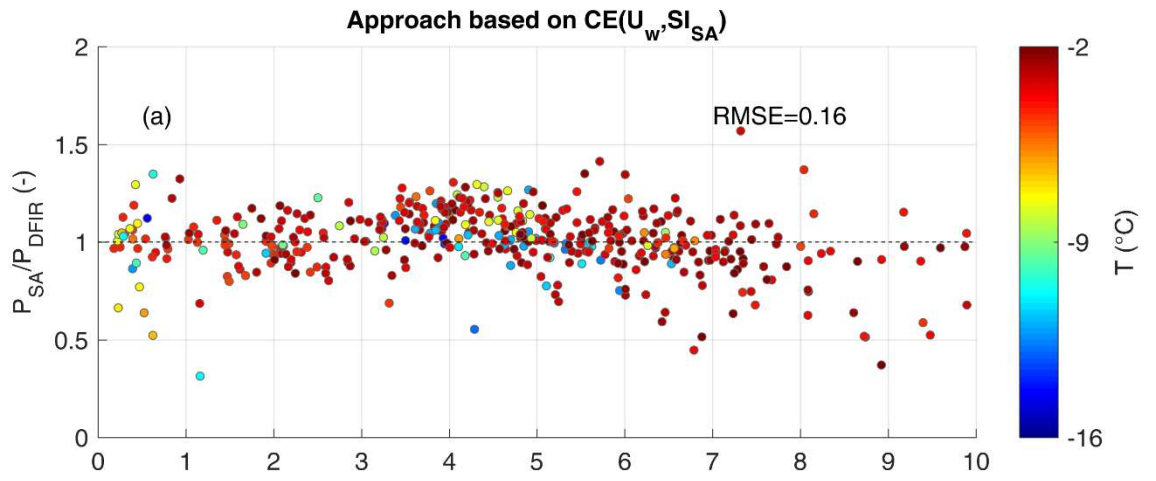


Figure 6: Residuals of  $CE = P_{SA} / P_{DFIR}$  obtained after correcting the 30-min single AlterSA shielded snow gauge measurements from the CARE (Canada) field test site using Equation 3 (top panel) and Equation 12 (bottom panel), with the associated RMSE values. Residuals are colour coded according to the environmental temperature  $T$  (top panel) and the snowfall intensity  $SI_{SA}$  (bottom panel).



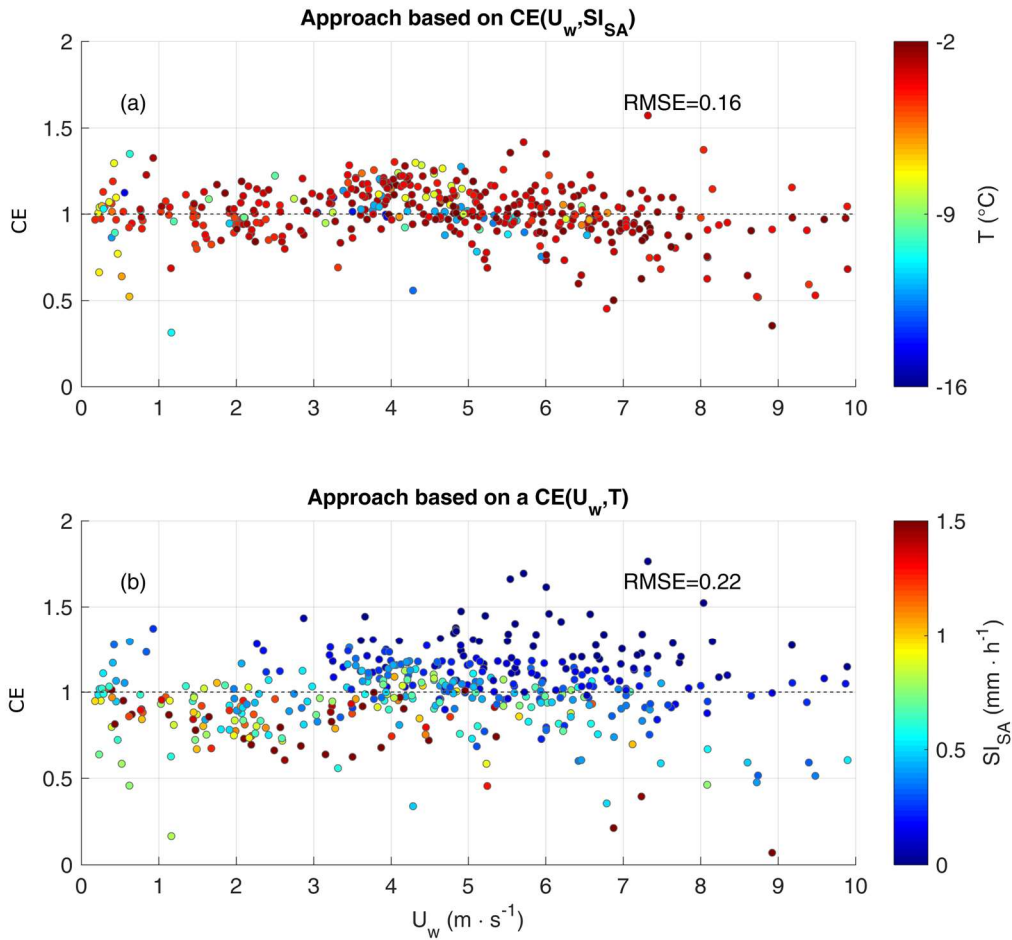


Figure 7: Residuals of  $CE = P_{SA} / P_{DFIR}$  obtained after correcting the 30-min single AlterSA shielded snow gauge measurements from the Haukeliseter (Norway) field test site using Equation 3 (top panel) and Equation 12 (bottom panel), with the associated RMSE values. Residuals are colour coded according to the environmental temperature  $T$  (top panel) and the snowfall intensity  $SI_{SA}$  (bottom panel).

5

#### 4 Sensitivity to the time aggregation

The analysis of field data proposed in section 3 has been repeated on the 1-min measurements performed by the single AlterSA shielded gauge at the Marshall field test site from January 2013 to April 2015 and aggregated over time intervals equal to 5, 10, 30 and 60 min. The regression coefficients obtained by applying the inverse exponential laws functions described by equations 12 and 3 are reported in Table 23. Figure 8 shows the CE specified curves calculated for different measured snowfall

10

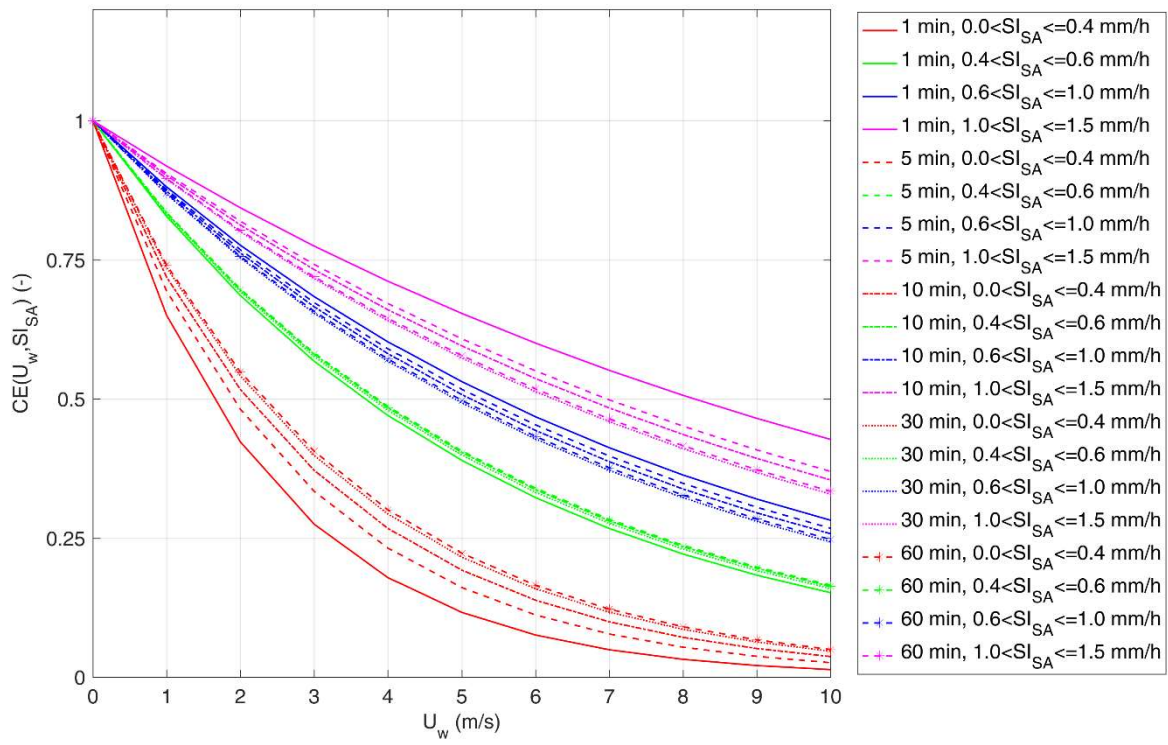
intensities  $SI_{SA}$  and time resolutions  $\Delta t$ . In all cases, a strong  $CE$  dependency on  $SI_{SA}$  draws distinct variations with wind speed, which do not overlap with each other. On the other hand, measurements made with a 30-min sampling interval provide  $CE$  curves that are closer to each other, and hence slightly less influenced by the measured [snowfall intensity  \$SI\$](#) , but still significantly different. This is partially explained by the fact that  $SI_{SA}$  is strongly [timeaggregation](#) dependent and when the

5 intensity measurements are averaged over a large time interval they become less representative of the internal variability. The representativeness of the proposed  $CE(U_w, T)$  transfer functions (represented by their linear correlation coefficient  $r$  in Table [23](#)) with respect to the field measurements decreases sharply below 5 minutes for temperature, while it doesn't for  $CE(U_w, SI_{SA})$ , suggesting that the  $T$  dependence becomes weaker at high resolution while the  $SI_{SA}$  dependence not so much. A similar behaviour is reported [byin](#) Table [34](#) in terms of  $RMSE$ , where the transition between the 5-min and the 1-min

10 aggregation intervals yields the larger  $RMSE$  increase for the  $CE(U_w, T)$  formulation. Therefore, the  $SI_{SA}$ -dependence [on  \$SI\_{SA}\$](#)  is more robust with respect to time aggregation. As shown in section 3, [WMO-SPICE](#) used a 30-min [periodaggregation interval](#) to assess [the  \$CE\$](#) , which still show significant variability at [any](#) given wind speed.

15 **Table 23:** Coefficients ( $a$ ,  $b$  and  $c$ ) of the inverse exponential function fitted at various aggregation intervals for the  $CE(U_w, T)$  and  $CE(U_w, SI_{SA})$  formulations, [with the associated](#) linear correlation coefficient ( $r$ ), and number of [periodsdata](#) available ( $n$ ). The calculation used measurements made by [single-Afterthe SA shielded](#) gauge at the Marshall field [test](#) site from January 2013 to April 2015.

$\Delta t$ (min)	$CE(U_w, T)$			$r$	$CE(U_w, SI_{SA})$			$r$	$n$
	$a$ (-)	$b$ (-)	$c$ (-)		$a$ (-)	$b$ (-)	$c$ (-)		
1	0.0588	0.6575	1.0502	0.60	18.0058	213.0772	0.5717	0.87	6943
5	0.0539	0.7155	1.1036	0.75	1.8436	27.9843	0.5957	0.90	1405
10	0.0500	1.1350	1.1648	0.81	0.4372	6.5754	0.6851	0.91	697
30	0.0555	0.9313	0.8761	0.85	0.3141	4.8702	0.7596	0.94	226
60	0.0539	1.0996	0.9338	0.87	0.2985	4.6410	0.7649	0.95	115



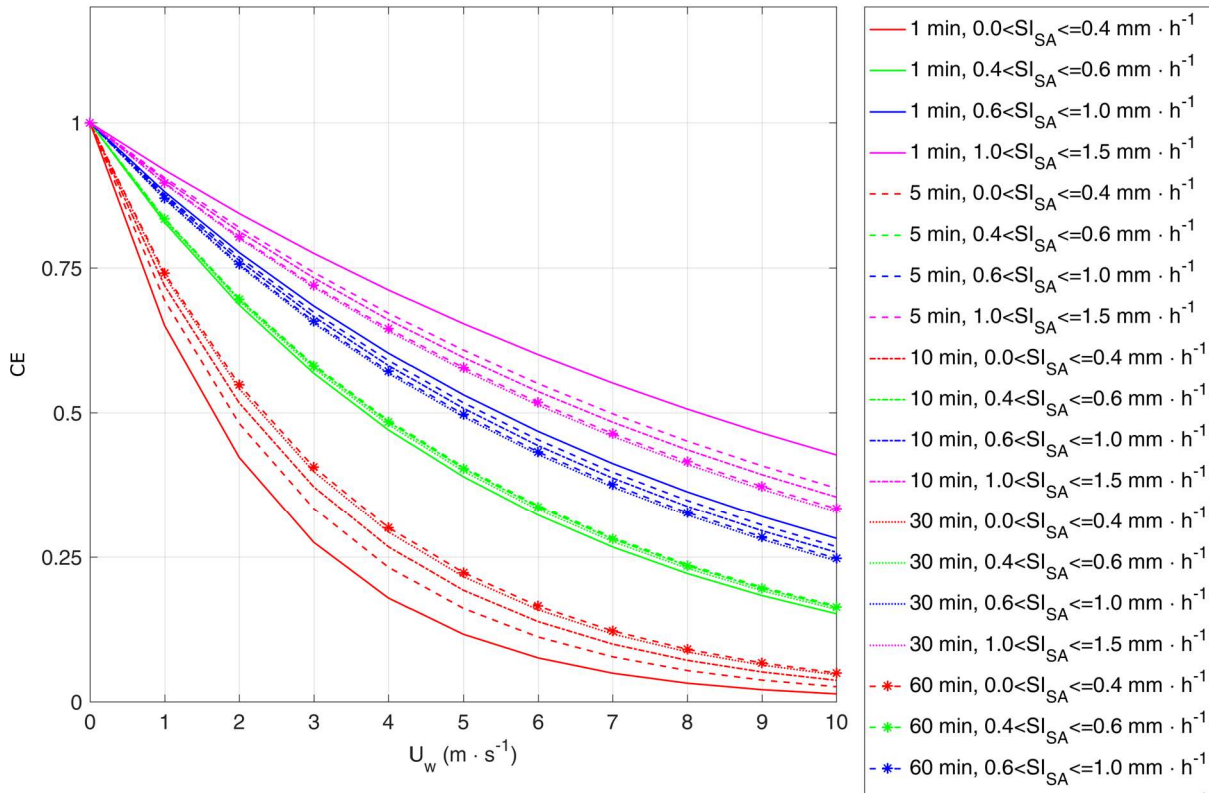


Figure 8: Collection efficiency Best-fit  $CE(U_w, SI)$  curves of the single AlterSA shielded snow gauge at the Marshall field site at 1, 5, 10, 30 and 60-min sampling intervals (different line types) grouped by the measured snowfall intensity-SI (different line colors).

5 Figure 8 demonstrates that the 10-min time interval may represent a trade-off point between the availability of correlated  $SI_{SA}$  and  $CE$  observations and the need of accumulating significant amounts of snowfall when lower aggregating the measurement over a longer interval during low precipitation intensities occur intensity. An evaluation of the impact of the data integration time on the correction of the  $P_{SA}$  observations was made by considering snowfall accumulations computed fromat different periods aggregation intervals. Table 34 shows that a larger dispersion of the CE of the corrected wind induced measurements (quantified by the root mean squared error RMSE) around the optimal value ( $CE=1$ ) is observed when smaller time periods short aggregation intervals are considered. Table 34 also shows that smaller  $RMSEs$  are systematically observed when the CE is calculated using the measured snowfall intensity-On the other hand SI. Indeed, shorter time aggregation intervals show yield a larger improvement of the correction when using the measured snowfall intensity SI rather than temperature, as demonstrated by larger values of the difference  $\Delta RMSE = RMSE(CE(U_w, T)) - RMSE(CE(U_w, SI))$ . This is a consequence of the increasingly

10 better fit of the  $CE(U_w, SI_{SA})$  formulation with reducing the aggregation scale, as already shown in Table 2.

15

**Table 3: Root-mean-square-error4: RMSE of the solid-precipitation measurements made by the single AlterSA shielded gauge at the Marshall field test site over different timeaggregation intervals  $\Delta t$  byafter applying athe correction based on snowfall-intensitySI,  $CE(U_w, SI_{SA})$ , and air temperature,  $CE(U_w, T)$ , and their difference  $\Delta RMSE$ .**

$\Delta t$ (min)	RMSE ( $CE(U_w, T)$ ) (-)	RMSE ( $CE(U_w, SI_{SA})$ ) (-)	$\Delta RMSE$ (-)
1	0.26	0.16	0.10
5	0.19	0.12	0.07
10	0.16	0.11	0.05
30	0.13	0.08	0.04
60	0.12	0.07	0.05

The fact that the amount of scatter reduction  $\Delta RMSE$  increases with shorter accumulation-timeaggregation intervals, seems to support the need of high-resolution measurements to improve the accuracy of the snow data. For instance, the scatter resulting from the correction of 30-min accumulation measurements based on wind speed and temperature can be achieved for a 10-min accumulation measurements if the snowfall-intensitySI is used for the correction. Thus by using the SI in the transfer function instead of temperature, one can either achieve a higher skillskill for a given aggregation time period-of-accumulation or achieve a higher time-resolutionaggregation interval with RSEa RMSE similar to the one traditionally obtained for a longer time period by including the snowfall intensity in the transfer functionaggregation interval.

## 5. CFD Validationsimulation and validation

The following section presents the CFD modelling framework used to compare to the observations in section 3 and to validate the physical basis of using the SI as an explanatory variable for the CE.

### 5.1 Airflow modelling and CE calculation

The flow field around a SA shielded gauge was numerically simulated using the Open Foam software and is described by Colli et al. (2015). The time-averaged air velocity, turbulent kinetic energy and pressure fields were solved by means of a Reynolds Averaged Navier-Stokes k- $\omega$  SST model.

The trajectories of drysnow particles falling through the CFD flow field are calculated using a Lagrangian model (Colli et al. 2015) for wind speeds between 1 and 8 m/s. The particle characteristics are from Rasmussen et al. (1999).

Several particle sizes were simulated to capture the dependence of  $CE$  on particle size. The PSD of snowfall events can be described using the gamma distribution, as shown by Brandes et al. (2007), which is similar than Marshall and Palmer (1948) but with a shape parameter.:

$$N(D) = N_0 \cdot D^\mu \cdot D^{-\lambda \cdot D} \quad (4)$$

5 where  $D$  is the snowflake diameter,  $N_0$  is the scale parameter,  $\mu$  characterizes the curvature and  $\lambda$  the slope of the distribution. According to Brandes et al. (2007)  $\mu$  can be estimated by the following expression:  $\mu = -0.00499 \lambda^2 + 0.798 \lambda - 0.666$ . In this work we adopted a general intercept value equal to  $N_0 = 1.5 \cdot 10^6 \text{ mm}^{-1} \text{ m}^{-3}$  and, based on observations, the slope parameters used are  $0.5 \text{ mm}^{-1} < \lambda < 1.5 \text{ mm}^{-1}$  (Brandes et al., 2007; Houze et al., 1979). The estimation of  $CE$  is based on the particle counting technique described in Colli et al. (2016b), :

$$CE(U_w) = \frac{\int_0^{d_p^{max}} V_w(d_p) A_{inside}(d_p, U_w) N(d_p) d_p}{\int_0^{d_p^{max}} V_w(d_p) A_{gauge} N(d_p) d_p} \quad (5)$$

10 where  $A_{inside}(d_p, U_w)$  is the effective collecting area associated with the number of particles collected by the gauge and  $A_{gauge}(d_p, U_w)$  is the area associated with the entering particles in the case of undisturbed airflow. Finally,  $V_w(d_p)$  is the equivalent water volume.

## 15 **5.2 PSD and snowfall intensity collected by the gauge**

The CFD analysis performed by Thériault et al. (2012) found a physical explanation for the large variability of the gauge catch performance observed for a given  $U_w$  and a specific type of precipitation from variations in the particle size distribution. Colli et al. (2015) confirmed this conclusion by providing different  $CE(U_w)$  functions computed using an improved CFD approach corresponding to the slope parameter ( $\lambda$ ) equal to 0.25, 0.50 and  $1 \text{ mm}^{-1}$  (the same values used by Thériault et al. (2012)).

20 We expanded that work here and the collection efficiency results for a larger set of  $\lambda$ s and reference snowfall intensity values are reported computed based on the simulation and the slope of the size distribution is given in Table 4. The table 5. It shows that steeper PSD-slopes of the PSD (represented by higher  $\lambda$ ), and as a consequence smaller mean particle sizes, are characterized by lower values of the  $CE$ . This is due to the stronger influence of the airflow around the gauge collector on the trajectories of the smaller particles. The  $CE$  values calculated in Table 4 shows 5 show that the variability of  $CE$  for a given  $\lambda$  remains significant in all the simulations performed with a wind speed higher than  $3 \text{ m s}^{-1}$ .

**Table 45:** Ratio between the collected [snowfall intensity-SI](#) and the reference [snowfall intensity-SI \(mmh<sup>-1</sup>\)SI](#) by varying the wind speed  $U_w$  (m s<sup>-1</sup>) and the slope parameter  $\lambda$  (mm<sup>-1</sup>) of the [particle size distributionPSD](#).

$\lambda$	0.5	0.7	0.9	1.1	1.3	1.5	1.7	1.9
SI	8.49	3.86	2.1	1.26	0.81	0.54	0.38	0.27
$U_w= 1$ m/s	1	1	1	1	1	1	1	1
$U_w= 2$ m/s	0.97	0.97	0.97	0.97	0.97	0.97	0.97	0.97
$U_w= 3$ m/s	0.94	0.93	0.93	0.93	0.93	0.93	0.93	0.92
$U_w= 4$ m/s	0.87	0.86	0.85	0.84	0.84	0.83	0.82	0.81
$U_w= 5$ m/s	0.78	0.74	0.7	0.67	0.63	0.6	0.57	0.54
$U_w= 6$ m/s	0.69	0.61	0.54	0.47	0.41	0.35	0.31	0.27
$U_w= 7$ m/s	0.51	0.39	0.29	0.21	0.15	0.11	0.08	0.06
$U_w= 8$ m/s	0.32	0.19	0.11	0.06	0.03	0.02	0.01	0.01

5 [The CFD analysis performed by Thériault et al. \(2012\) found that the type of precipitation and their sizes explained some of the scatter in the gauge catch efficiency for a given  \$U\_w\$ . Colli et al. \(2015\) confirmed this conclusion by providing different  \$CE\(U\_w\)\$  functions as well as an improve drag coefficient using the same slope parameters \( \$\lambda= 0.25, 0.50\$  and  \$1 \text{ mm}^{-1}\$ \) as in Thériault et al. \(2012\).](#)

10 [To link the snowfall intensity with the PSD, an example of the simulated size distribution of dry snow particles that fall into the gauge is shown in Figure 9 for a sample precipitation characterized by  \$\lambda=1.0 \text{ mm}^{-1}\$  and  \$N\_0=10^6 \text{ mm}^{-1}\text{m}^{-3}\$ , as. These PSD parameters were suggested by Houze et al. \(1979\) who observed the snow size distribution in different atmospheric conditions. TheIn agreement with Figure 9 of Thériault et al. \(2012\), it is shown that the gauge starts missing the lower particle sizes when  \$U\_w\$  approaches  \$4 \text{ m s}^{-1}\$ , and higher wind speeds correspond to narrower ranges of  \$D\_p\$ particle diameters that are collected by the gauge \(and higher curvature parameter  \$\mu\$ \). This smaller particles fall in the gauge at  \$4 \text{ m/s}\$  than previously found by Thériault et al. \(2012\). This is probably due to the updated drag coefficient.](#)

15

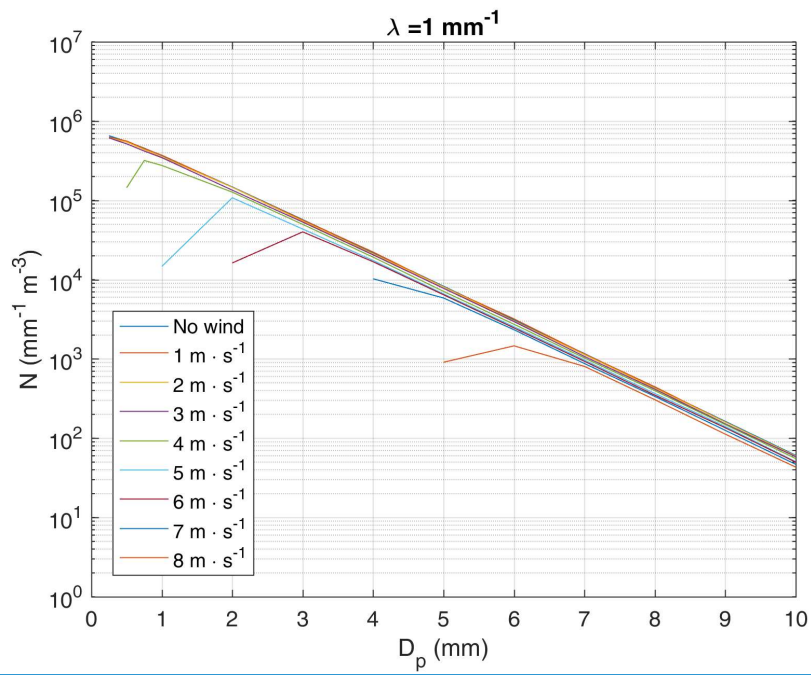
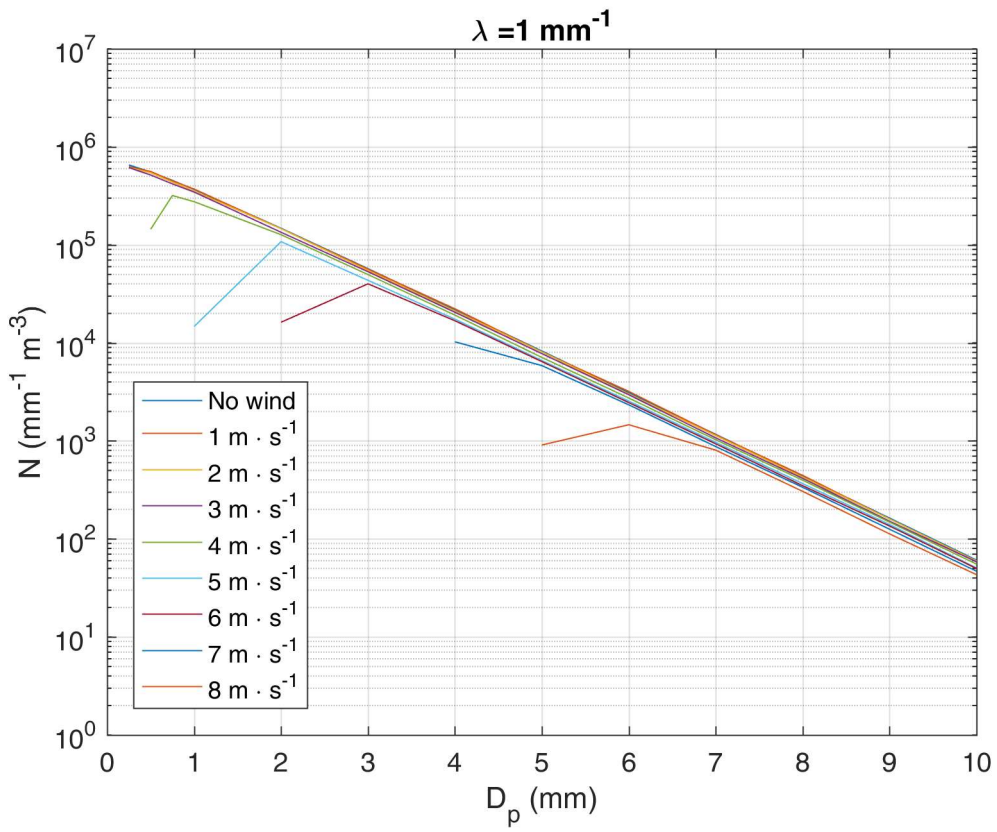


Figure 9: CFD simulated ~~particle size distributions  $N(D_p)$  PSD of solid precipitation dry snow~~ collected by the ~~single AlterSA shielded gauge under different wind conditions, using  $\lambda=1.0 \text{ mm}^{-1}$  and  $N_0=10^6 \text{ mm}^{-1}\text{m}^{-3}$~~

For ~~the larger  $D_p$  diameters~~, the PSD of the precipitation collected by the gauge maintains the same slope  $\lambda$  of the reference and slightly decrease the concentration number  $N_0$  with increasing  $U_w$ . The collected  $N(D_p)$  values are lower than the reference PSD but maintain the same order of magnitude. An exception is represented by the smaller diameter of the PSDs collected under wind speeds higher than  $4 \text{ m s}^{-1}$ . In this case, the  $N(D_p)$  value is approximately one order of magnitude lower than the reference one. ~~The wind-induced underestimation of the  $SI_{SA}$  for a given  $\lambda$  is due to the loss of high concentration small particles falling into the gauge.~~

~~The main consequence of the  $\lambda$  invariance is that the significant wind-induced underestimation of  $SI_{SA}$  reported by Table 4 is principally explained by the loss of high concentration small particles.~~

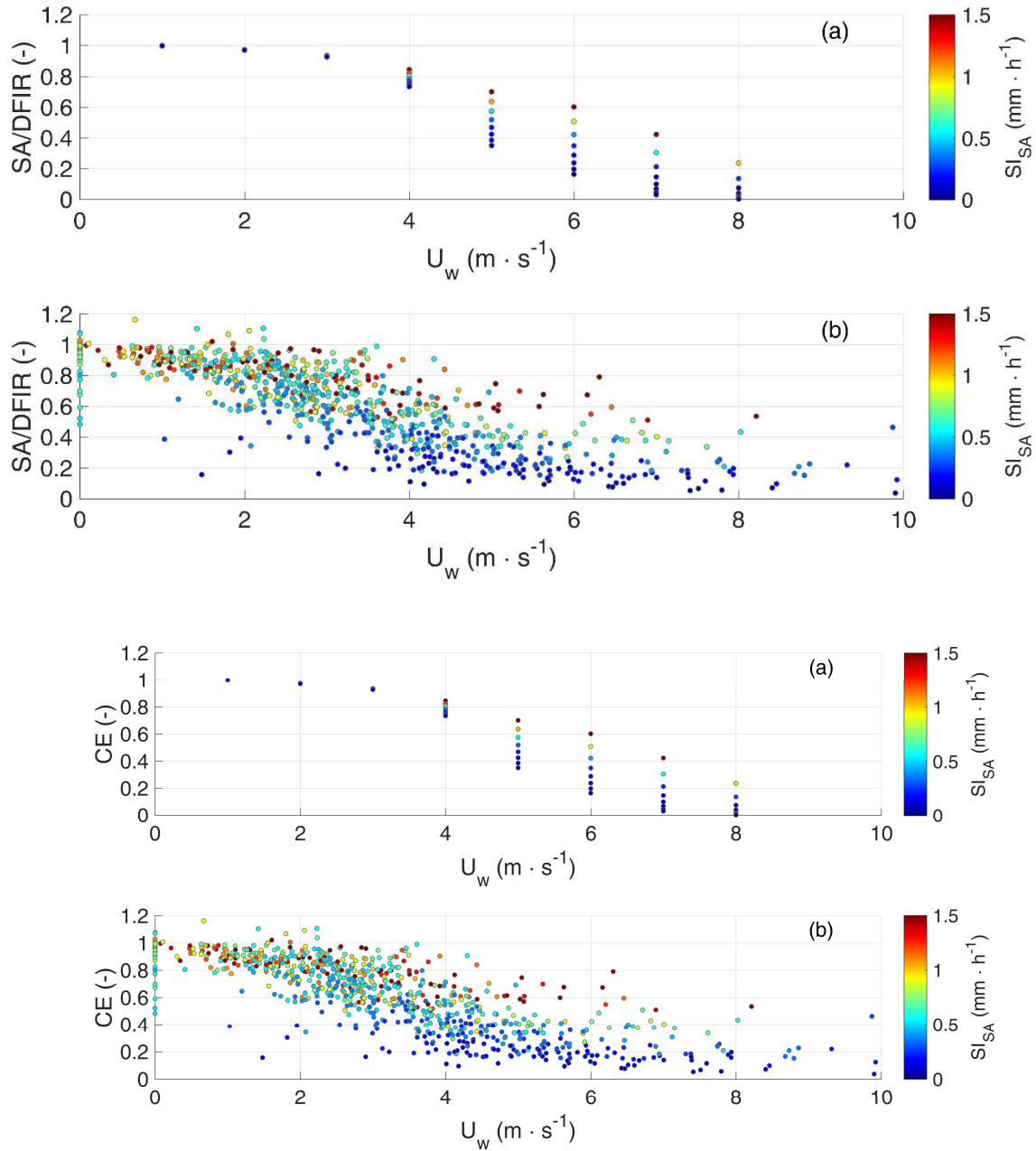
### 5.23 Comparing the results of field observations and CFD simulations

The computed  $CE$  variation with wind speed ~~for the different snowfall intensities as a function of  $SI$~~  is shown in Figure 10. ~~The Marshall field site measurements are reported in Fig. 10b while the~~ The results of the CFD trajectory analysis are shown in ~~Fig. Figure 10a while the Marshall field site measurements are reported in Figure 10b.~~ The plot is comparable to Figure 8 of Colli et al (2015) where the correlation between the simulated ~~collection efficiency  $CE$~~  and the ~~particle size distribution PSD~~ was discussed. For ~~any~~ given  $U_w$  wind speed, a set of eight ~~collection efficiency points  $CE$  values~~ have been computed according to the slope  $\lambda$  of the reference ~~particle size distribution PSD~~, which is correlated with the ~~snowfall intensity  $SI$~~  measured by the gauge (equation 21).

The CFD results show that when  $U_w$  the wind speed is higher than  $3 \text{ m s}^{-1}$ , there is an abrupt increase of the  ~~$P_{SA}/P_{DFIR}$  scattering  $CE$  scatter~~ from  $1 \text{ mm h}^{-1} < SI_{SA} < 1.5 \text{ mm h}^{-1}$  (red points) to  $0 \text{ mm h}^{-1} < SI_{SA} < 0.5 \text{ mm h}^{-1}$  (blue points), associated with a decrease of the ~~collection efficiency  $CE$~~  at a given wind speed (Fig. Figure 10a). When the average wind speed is lower or equal to  $3 \text{ m/s}$  the dependency of the  ~~$P_{SA}/P_{DFIR}$   $CE$~~  on the measured ~~snowfall intensity  $SI$~~  becomes less significant, meaning that even the smaller particles are mostly collected by the ~~single AlterSA shielded gauge~~. The latter result is not confirmed by the field measurements provided in Figure 1 that show a persistent scattering of  ~~$P_{SA}/P_{DFIR}$  the  $CE$  even~~ at the lower wind speeds. Such behaviour has been already explained by Colli et al. (2016b) that demonstrated the role of the airflow turbulence generated by the wind shield in the ~~collection efficiency  $CE$~~  scattering by means of time-dependent CFD simulation. ~~The same figures are not obtained by using time averaged CFD simulations that do not represent the airflow time fluctuations, leading to the  $P_{SA}/P_{DFIR}$  distribution of Figure 10.~~

The results of the CFD simulations therefore highlight the physical dependency between the ~~collection efficiency  $CE$~~  and the ~~snowfall intensity  $SI$~~  measured by the gauge, and this dependency varies according to the wind speed. Figure 10b shows the

CE field observations for [the 10-min accumulation-timeaggregation interval dataset](#), categorized by [snowfall-intensity](#)  $SI$  confirming the dependency between collected precipitation, measured intensity and wind speed.

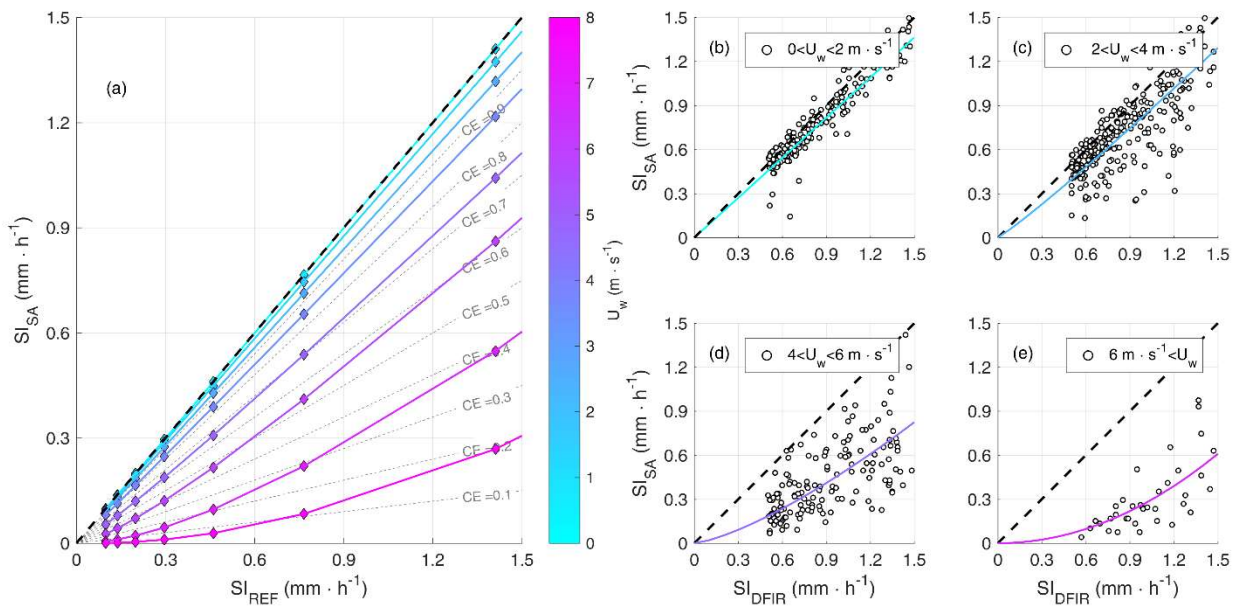


5 Figure 10: [Collection efficiency  \$CE = P\_{SA}/P\_{DFIR}\$  scatter](#) of the 10-min [single AlterSA shielded](#) gauge measurements simulated by means of the time-averaged CFD model (panel a) and [actual 10-min field](#) measurements (panel b) made at the Marshall field [test site](#) (CO, USA). Data are colour coded according to the measured [snowfall intensity  \$SI\_{SA}\$](#) , showing [SI](#).

The added value of using the clustering of the measurements.

The conceptual improvement achieved when the  $SI$  in the transfer function is parameterised according to the measured snowfall intensity is best visualised in the  $SI_{SA}$  vs.  $SI_{REF}$  scatter plot shown in Figure 11a, where  $SI_{REF}$  is the reference snowfall intensity  $SI$  (assumed coincident with  $SI_{DFIR}$  for the field data). In this graph, where the wind speed is colour-coded according to the side bar, the iso-CE lines would be linear (grey dotted lines) in the absence of a clear influence of the  $SI_{SA}$  on the collection efficiency. However, this is not supported neither by the field data (white dots in panels b, c, d, e of Figure 11) nor by numerical simulations (solid coloured curves and diamonds in Figure 11a). Instead, a CE. A clear deviation from linearity is observed, showing that the collection efficiency increases far beyond linearity with the measured snowfall intensity,  $SI_{SA}$ , for  $SI$  at any given wind speed class. This deviation vanishes when  $U_w \rightarrow 0$  and increases with the wind speed, therefore justifying the larger spread of collection efficiency CE values observed towards the right-hand side in of Figure 10 (a and b).

15



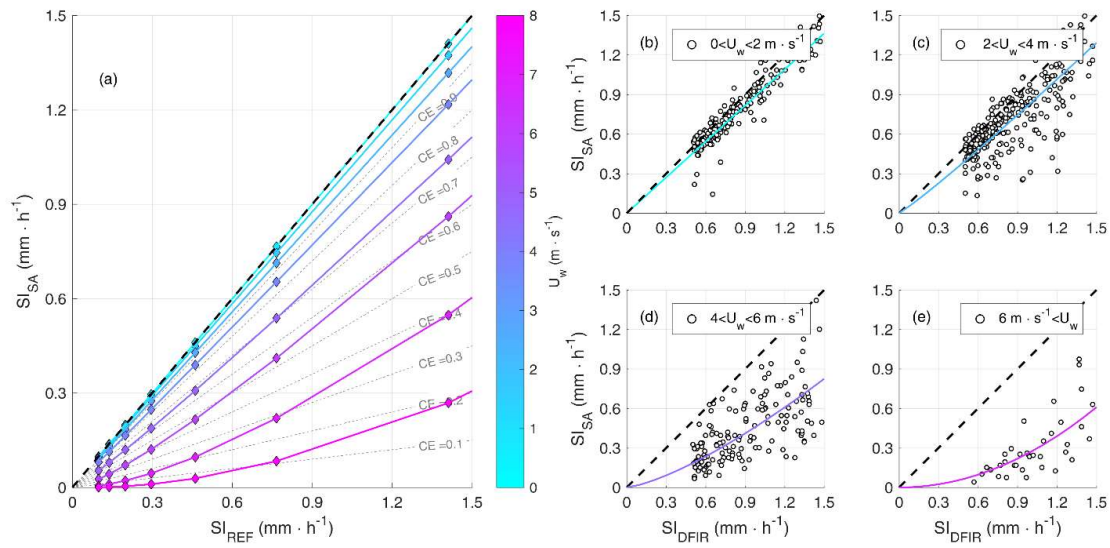


Figure 11: **Collection efficiency deviation** from linearity of the CE (grey dotted lines) in (a) when increasing the wind speed (colour coded according to the side bar) in the measured  $SI_{SA}$  vs. reference  $SI_{REF}$  snowfall intensity  $SI$  plane. The deviation is evident in both the results of numerical simulation (solid coloured lines and diamonds in panel a) and field data (white circles in panels b, c, d, e) although with some residual dispersion/scatter. The field data is presented together with the  $SI_{SA} = aSI_{DFIR}^b$  power law regressions performed for the  $U_w < 2 \text{ ms}^{-1}$  ( $a=0.90, b=1.00, r=0.98$ ),  $2 < U_w < 4 \text{ ms}^{-1}$  ( $a=0.83, b=1.08, r=0.94$ ),  $4 < U_w < 6 \text{ ms}^{-1}$  ( $a=0.47, b=1.37, r=0.84$ ) and  $6 \text{ ms}^{-1} < U_w$  ( $a=0.27, b=2.00, r=0.85$ ) various wind speed classes.

## 6 Conclusions

The present analysis of recent WMO–SPICE quality controlled 30–min accumulation data from the Marshall field-test site (CO, USA) revealed that the wind-induced undercatch of solid precipitation gauges is best correlated with the measured snowfall intensity, rather than temperature, in addition to wind speed. While the environmental temperature provides general relevant information about whether the precipitation is rain (Auer, 1974), wet or dry snow (Rasmussen et al., 1999) it is not clear how the exact type of solid precipitation can be easily determined in the field. At cold temperatures, which are often associated with dry snow, it is also possible to observe rime particles that would have higher collection efficiency (Thériault et al., 2012). On the other hand, the measured snowfall intensity has the advantage of including information about the PSD (Pruppacher and Klett, 1997). Optimal curve fitting used to derive the transfer function for the GEONOR gauge in a single Alter shield and in a DFIR configuration indicates that accounting for snowfall intensity indeed reduces the scatter of the residuals.

This result is confirmed by the analysis of data from other field sites, such as CARE (Canada) and Haukeliseter (Norway), and shows a consistent behaviour under different climatological conditions. Recent results from Chubb et al. (2015) found

improved under-catch correction for an ETI weighing gauge for data collected in the Snowy Mountains of Australia. This supports our results and suggests that other snow gauges can benefit from this type of adjustment.

The physical basis for the improved parameterisation of the transfer function by using the measured [snowfall intensity  \$SI\$](#)  was shown through CFD modelling of the gauge snow collection process to be due to the correlation of large particles with high intensities. Large particles are preferentially collected by a snow gauge, even in strong wind, due to their higher fall velocity, allowing them to break through streamlines of flow above the gauge and be collected. The CFD modelling was able to reproduce the [collection efficiency  \$CE\$](#)  pattern observed in the field providing strong evidence of the hypothesized behaviour.

The analysis of the optimal [accumulation period aggregation interval](#) of the snowfall measurements was based on the evaluation of the residual data scattering after applying [a correction adjustments](#) based on wind speed  $U_w$  and [either](#) environmental temperature  $T$  and [a correction based on  \$U\_w\$  and/or](#) the measured [snowfall intensity  \$SI\_{S,4}\$](#) . It has been observed that shorter accumulation intervals increase the dependency of [the  \$CE\$](#)  on [the  \$SI\_{S,4}\$](#)  and a stronger benefit in using the proposed approach. On the other hand, it was also observed [that](#) larger accumulation intervals are generally associated with a smaller residual scattering of the measurements. According to our analysis, the 10-min [time aggregation](#) interval may represent a trade-off point between the availability of correlated [the  \$SI\_{S,4}\$](#)  and  $CE$  observations and the need of accumulating significant amounts of snowfall when lower precipitation intensities occur.

Overall, these findings provide an attractive method to improve operational measurements since no additional instrument, except for a wind sensor, is required to [derive the derived the improved adjusted](#) estimates of snow accumulation.

## 20 Acknowledgements

J.M Thériault [was](#) funded by the Natural [Sciences and Engineering](#) Research Council ([NSERC](#)) of Canada ([NSERC](#)).

## References

- 25 Alter, J.: Shielded storage precipitation gages. *Mon. Wea. Rev.*, 65, 262–265, 1937.
- [Auer, A. H.: The rain versus snow threshold temperature. \*Weatherwise\*, 27, 67 \(2\), 1974.](#)
- [Brandes, E. A., Ikeda, K., Zhang, G., Schönhuber, M., & Rasmussen, R. M.: A statistical and physical description of hydrometeor distributions in Colorado snowstorms using a video disdrometer. \*Journal of applied meteorology and climatology\*, 46\(5\), 634-650, 2007.](#)
- 30 Buisán, S. T., Earle, M. E., Collado, J. L., Kochendorfer, J., Alastrué, J., Wolff, M., Smith, C. D., and López-Moreno, J. I.: Assessment of snowfall accumulation underestimation by tipping bucket gauges in the Spanish operational network, *Atmos. Meas. Tech.*, 10, 1079-1091, 2016.

- Chubb, T., M.J. Manton, S.T. Siems, A.D. Peace, and Bilish, S.P.: Estimation of Wind-Induced Losses from a Precipitation Gauge Network in the Australian Snowy Mountains. *J. Hydrometeorol.*, 16, 2619–2638, 2015.
- Colli, M., R. Rasmussen, J.M. Thériault, L.G. Lanza, C.B. Baker, and Kochendorfer J.: An Improved Trajectory Model to Evaluate the Collection Performance of Snow Gauges. *J. Appl. Meteor. Climatol.*, 54, 1826–1836, 2015.
- 5 Colli, M., Lanza, L.G., Rasmussen, R.M. and ~~Thériault~~Thériault, J.M.: The collection efficiency of shielded and unshielded precipitation gauges. Part I: CFD airflow modelling. *J. of Hydrometeorol.*, 17(1), pages 231-243, 2016a.
- Colli, M., Lanza, L.G., Rasmussen, R.M. and ~~Thériault~~Thériault, J.M.: The collection efficiency of shielded and unshielded precipitation gauges. Part II: modelling particle trajectories. *J. of Hydrometeorol.*, 17(1), 245-255, 2016b.
- 10 Constantinescu, S., Krajewski, W., Ozdemir, C., Tokyay, T.: Simulation of flow around raingauges: Comparison of LES with RANS models. *Journal of Advances in Water Resources* 30, 43–58, 2006.
- Eldred, M.S., Agarwal, H., Perez, V.M., Wojtkiewicz, S.F., Jr., and Renaud, J.E.: Investigation of Reliability Method Formulations in DAKOTA/UQ, *Structure & Infrastructure Engineering: Maintenance, Management, Life-Cycle Design & Performance*, Vol. 3, No. 3, pp. 199-213, 2007.
- 15 Folland, C. K.: Numerical models of the raingauge exposure problem, field experiments and an improved collector design. *Q.J.R. Meteorol. Soc.*, 114: 1485-1516, 1988.
- Gergely M. and Garrett,T.J.: Impact of the natural variability in snowflake diameter, aspect ratio, and orientation on modeled snowfall radar reflectivity. *J. Geophys. Research*, 121(20), 12,236-12,252, 2016.
- Goodison, B., P. Louie, and Yang, D.: WMO solid precipitation measurement intercomparison: final report. WMO Tech. Document 872, World Meteorological Organization, Geneva, Switzerland, 1998.
- 20 Houze, R. A., P. V. Hobbs, and Herzegh,P.H.: Size distributions of precipitation particles in frontal clouds. *J. Atmos. Sci.*, 36, 156–162, 1979.
- Kochendorfer, J., Rasmussen, R., Wolff, M., Baker, B., Hall, M. E., Meyers, T., Landolt, S., Jachcik, A., Isaksen, K., Brækkan, R., and Leeper, R.: The quantification and correction of wind-induced precipitation measurement errors, *Hydrol. Earth Syst. Sci.*, 21, 1973-1989, 2017a.
- 25 Kochendorfer, J., Nitu, R., Wolff, M., Mekis, E., Rasmussen, R., Baker, B., Earle, M. E., Reverdin, A., Wong, K., Smith, C. D., Yang, D., Roulet, Y.-A., Buisan, S., Laine, T., Lee, G., Aceituno, J. L. C., Alastrué, J., Isaksen, K., Meyers, T., Brækkan, R., Landolt, S., Jachcik, A., and Poikonen, A.: Analysis of single-Alter-shielded and unshielded measurements of mixed and solid precipitation from WMO-SPICE, *Hydrol. Earth Syst. Sci.*, 21, 3525-3542, 2017b.
- 30 Kochendorfer, J., Nitu, R., Wolff, M., E. Mekis, R. Rasmussen, B. Baker and others: Testing and Development of Transfer Functions for Weighing Precipitation Gauges in WMO-SPICE. *Journal of Hydrology and Earth System Sciences Discussions*, 2017, 1-25, 2017c.
- Matrosov, S.Y., C. Campbell, D. Kingsmill, and E. Sukovich: Assessing Snowfall Rates from X-Band Radar Reflectivity Measurements. *J. Atmos. Oceanic Technol.*, 26, 2324–2339, 2009.
- [Marshall, J.S. and W.M. Palmer: The distribution of raindrops with size. \*J. Meteor.\*, 5, 165–166, 1948.](#)
- 35 Nespor, V., and B. Sevruk: Estimation of wind-induced error of rainfall gauge measurements using a numerical simulation. *J. Atmos. Oceanic Technol.*, 16 (4), 450–464, 1999.

- 5 Nitu, R., ~~and Coauthors:~~ Rasmussen, R., Baker, B., Lanzinger, E., Joe, P., Yang, D., Smith, C., Roulet, Y.A., Goodison, B., Liang, H., Sabatini, F., Kochendorfer, J., Wolff, M., Hendrikx, J., Vuerich, E., Lanza, L.G., Aulamo, O., Vuglinsky, V.: WMO intercomparison of instruments and methods for the measurement of solid precipitation and snow on the ground: Organization of the experiment. Preprints, TECO-2012: WMO Technical Conference on Meteorological and Environmental Instruments and Methods of Observations, Brussels, Belgium, WMO, 10 pp., 2012.
- 10 ~~Rasmussen and Coauthors:~~ Nitu, R., Roulet, Y.A., Wolff, M., Earle, M., Reverdin, A., C. Smith, C., Kochendorfer, J., Morin, S., Rasmussen, R., Wong, K., Alastrué, J., Arnold, L., Baker, B., Buisán, S., Collado, J.L., Colli, M., Collins, B., Gaydos, A., Hannula, H.-R., Hoover, J., Joe, P., Kontu, A. Laine, T., Lanza, L., Lanzinger, E., Lee, G.W., Lejeune, Y., Leppänen, L., Mekis, E., Panel, J.-M., Poikonen, A., Ryu, S., Sabatini, F., Thériault, J., Yang, D., Genthon, C., van den Heuvel, F., Hirasawa, N., Konishi, H., Nishimura, K., Senese, A.: WMO Solid Precipitation Intercomparison Experiment (SPICE) (2012 - 2015), Instruments and Observing Methods Report No. 131, 2018.
- 15 ~~Pruppacher, H.R. and Klett J.D.:~~ Microphysics of Clouds and Precipitation, Atmospheric and Oceanographic Sciences Library, Springer Netherlands, 954 pp., 2010.
- Rasmussen, R.M., J. Vivekanandan, J. Cole, B. Myers, and Masters C.: The Estimation of Snowfall Rate Using Visibility. *J. Appl. Meteor.*, 38, 1542–1563, 1999.
- 20 ~~Rasmussen, R., B. Baker, J. Kochendorfer, T. Meyers, S. Landolt, A.P. Fischer, J. Black, J.M. Thériault, P. Kucera, D. Gochis, C. Smith, R. Nitu, M. Hall, K. Ikeda, and Gutmann E.:~~ How well are we measuring snow: The NOAA/FAA/NCAR winter precipitation test bed. *Bull. Amer. Meteor. Soc.*, 93, 811–829, 2012.
- 25 Reverdin, A.: Description of the Quality Control and Event Selection Procedures used within the WMO-SPICE project, Madrid, Spain, September, 2016.
- Thériault, J., Rasmussen, R., Ikeda, K., Landolt, S.: Dependence of snow gauge collection efficiency on snowflake characteristics. *Journal of Applied Meteorology and Climatology* 51, 745–762, 2012.
- Thériault, J.M., R. Rasmussen, E. Petro, J. Trépanier, M. Colli, and Lanza, L.G.: Impact of Wind Direction, Wind Speed, and Particle Characteristics on the Collection Efficiency of the Double Fence Intercomparison Reference. *J. Appl. Meteor. Climatol.*, 54, 1918–1930, 2015.
- Thom, A. S.: Momentum, mass and heat exchange of plant communities, in: *Vegetation and the Atmosphere*, Vol. 1, edited by: Monteith, J. L., Academic Press, London, 1975.
- 30 Wolff, M., K. Isaksen, A. Petersen-Øverleir, K. Ødemark, T. Reitan, and Bækkan R.: Derivation of a new continuous adjustment function for correcting wind-induced loss of solid precipitation: results of a norwegian field study. *Hydrol. Earth Syst. Sci.*, 9(11), 10 043–10 084, 2014.
- ~~Yang, D., and Coauthors:~~ WMO: Guide to Meteorological Instruments and Methods of Observation, World Meteorological Organization Pub. N. 8, 2014 (updated 2017), ISBN 978-92-63-10008-5.
- 35 ~~Yang, D., and Goodison, B. E., Metcalfe, J. R., Louie, P., Leavesley, G., Emerson, D., Hanson, C. L., Golubev, V. S., Elomaa, E., Gunther, T., Pangburn, T., Kang, E. and Milkovic, J.:~~ Quantification of precipitation measurement discontinuity induced by wind shields on national gauges. *Water Resour. Res.*, 35 (2), 491508, 1999.